



Oligocene source and reservoir rocks evaluation using a multi-disciplinary approach within eastern offshore Nile Delta province



Mohamed Saad Elokazy ^{1*}, Mahmoud Yousry Zein El Din ² and Aymen Mostafa Morshedy ³

¹ Egyptian Natural Gas Holding Company EGAS, Egypt

² Geology department- Faculty of science- Al-Azhar University, Egypt

³ Petrosannan Petroleum Company, Egypt

NILE Delta Basin in the Eastern Mediterranean has been one of the most important hydrocarbon areas, with estimated undiscovered natural gas reserves 800+ trillion cubic feet. In favor of increasing certainty and giving the current study more confidence, a multi-disciplinary approach was applied to evaluate the Oligocene potentiality as a hydrocarbon source and reservoir by integrating Sequence stratigraphy concept, petrophysical evaluation and Basin modeling workflow.

Interpreting sequence stratigraphy framework would explain the spatial and temporal distribution of reservoir along the study area and consider the effect of various deposition process and depositional elements. On the other hand, petrophysical evaluation sheds light on the reservoir quality and track the changes of reservoir criteria and facies and proves that the effective porosity values directly affected by overburden thickness, average effective porosity in the shallowest cycle Ch_B is 15 % decreasing to 12% within the deeper cycle Ch_A and reached its lowest value 10% within the deepest cycle and maximum overburden. The turbidity channelized system - which is widely distributed in the region- and the predominant reservoirs of the Oligocene with wide range of reservoir thickness, from 1.6 m within Ch_B cycle at Helm-1st1 well location and reaches its maximum 68 m within Ch_B cycle at X-1 well location. In parallel with 1D basin modeling was applied as source rock evaluation technique to figure out the Oligocene source rock potentiality for hydrocarbon generation. A wide range of maturity levels marked, starting from the lowest mature source rock unit marked by low amount of total generated hydrocarbon 0.04 Mtone and recent critical moment 1.1 Ma within Ch_B cycle at Salamat-1 well location, to the most mature source rock unit with high amount of total generated hydrocarbon 0.74 Mtone with old critical moment 15.5 Ma within Ch_B cycle at Notus-1st2 well location. The results of this integrated work proved that, the Oligocene shale is the main source rock for both Oligocene and Miocene with total 1D generated hydrocarbon mass 4.84 Mton. Oligocene deposits proved a successful combined stratigraphical and structural hydrocarbon exploration play supported by various gas discoveries.

Keywords: Basin Modeling, Oligocene, East Mediterranean, Petrophysics.

1. Introduction

Egypt is divided into three main regions of significant petroleum provinces: the Gulf of Suez, the Western Desert, and the Nile Delta. The Nile Delta in Egypt stands out as a remarkable sedimentation system where the intricate relationship between the Nile River and the Mediterranean Sea has shaped its geological evolution for more than thirty-five million years, this area possesses distinctive geological characteristics, including specific sedimentation

patterns influenced by sediment transportation and subsequent diagenesis, (Abdel-Fattah, M.I., 2022). The present-day delta has passed through different events as part of the regional tectonics in the Mediterranean area, which has shaped many of its physiographic features. This area is now regarded as a major gas province and a promising area for future hydrocarbon exploration with increasing interest to many recent publications (El-Fakharani, A., & Abd

*Corresponding author e-mail: nourfouda@sci.asu.edu.eg

Received: 08/03/2025; Accepted: 04/04/2025

DOI: 10.21608/egjg.2025.365819.1103

©2025 National Information and Documentation Center (NIDOC)

El-Rahman, Y.2020, El-Sayed, A. M., & El Barkooky, A., 2023, Hassan, R. M., & Abdel-Fattah, M. I., 2023, Ismail et al., 2023; and Attia et al.,2024).

The Eastern Province, offshore the Nile Delta, represents the most important gas-producing provinces in Egypt as it located within the Eastern Mediterranean region with estimated undiscovered natural gas reserves with 800+ trillion cubic feet. (Schenk et al., 2021). Its main target reservoirs range from the Pleistocene (Wastani Formation) to the Cretaceous (carbonate build-ups), while thermogenic source rocks range from Jurassic, Cretaceous, to Oligocene time intervals, and active biogenic source rocks are found within Pliocene deposits. It contains a thick sequence of Paleogene-Quaternary clastics, which are considered to be prospective for hydrocarbons.

A multi-disciplinary approach lends a hand to modify the understanding of Oligocene petroleum system elements efficiency. A petrophysical evaluation technique was applied to quantitatively evaluate reservoir occurrence and ratio. Conducting a

chronostratigraphic correlation is a highly appreciated and valuable contribution to the scope of work; this will enable screening and tracking the change of petrophysical parameters along the study area (Fig. 1), which provides a regional understanding of the Oligocene reservoir quality and hydrocarbon accumulations. Delineating sequence stratigraphy surfaces and spatial distribution would enlighten the temporal understanding of depositional architecture, which would enhance reservoir facies tracking and give a new dimension to hydrocarbon exploration. Moreover, a source rock evaluation is applied to figure out the capability of deep-seated Oligocene strata to generate and expel hydrocarbons. 1D basin modelling would unlock the ability to evaluate the various petroleum system elements, determine at which depth the maturation phase commences sufficiently to expel hydrocarbons, and propose reservoir and seal deposits. Applying the 1D modelling technique to the five wells would give a clue about the spatial distribution of mature rocks and the maturation degree along the study area.

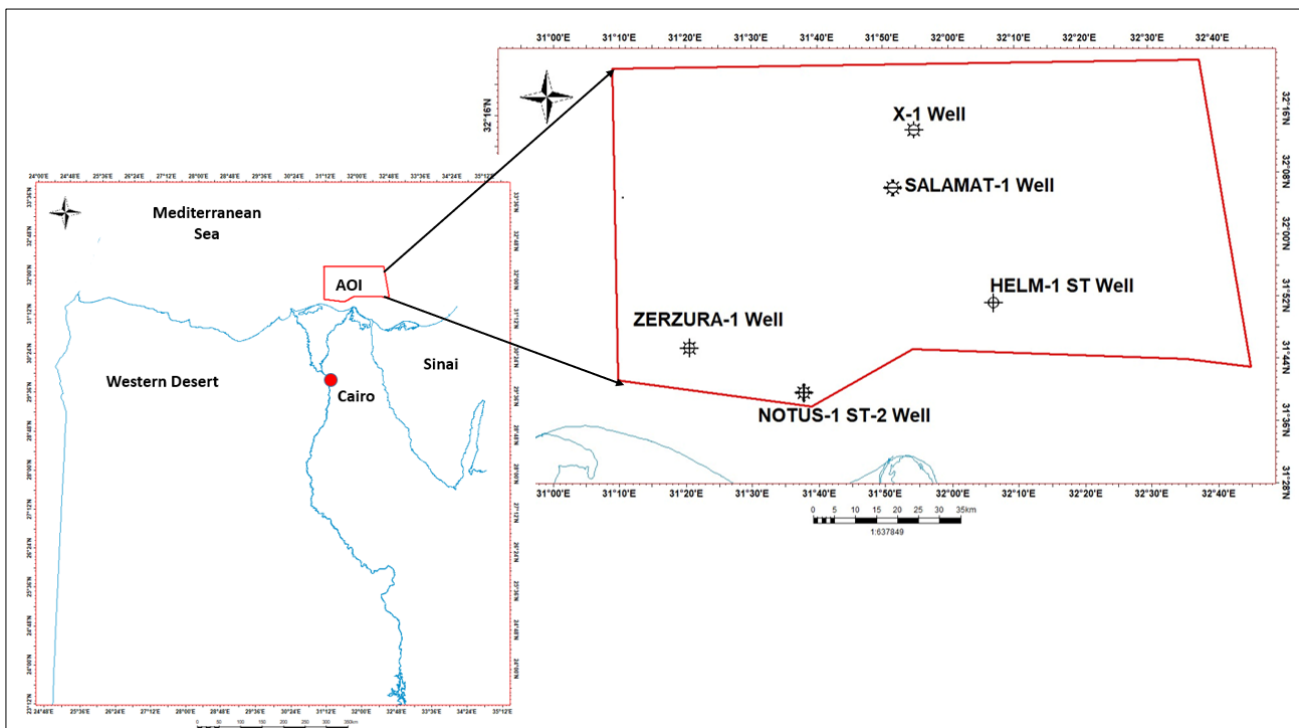


Fig. 1. Location map showing the study area and the wells in the study.

2 Geology and Lithostratigraphy of the area

The offshore Nile Delta exhibits three prominent structural characteristics within a triangular megastructure. To the south, it is bounded by an east-west trending fault known as the Hinge line, which separates the continental shelf to the south from the Nile Delta sedimentation system to the north. In the

west trending fault known as the Hinge line, which separates the continental shelf to the south from the Nile Delta sedimentation system to the north. In the

western Nile Delta, there is a significant slip fault running in a northeast-southwest direction, referred to as the Rosetta normal fault. This fault features a hanging wall to the southeast and a foot wall to the northwest, forming a substantial half-graben with a regional dip towards the southeast. The crest of this half-graben lies atop the Nile Delta offshore anticline (Nosjean, N., 2021). In the eastern Nile Delta, there is a major northwest-southeast strike-slip fault known as the Tamsah fault, which is the counterpart of the Rosetta fault. Along its hanging wall, it displays a series of productive parallel tilted fault blocks (Bentham, P.; 2011).

Along the course of geological history, both the onshore and offshore Nile Delta provinces have experienced a variety of geological events. The Tethyan rift border predominated the depositional processes from the Jurassic to the Early Cretaceous, forming the well-known Hinge Line that runs east-west and divides the northern and southern parts of the onshore Nile Delta Province. The shallow marine carbonates, Upper Jurassic, represent the oldest rock units penetrated in the Nile Delta Basin (Abdel Aal et al. 1994). The Cretaceous is subdivided into two parts: upper and lower. The Lower Cretaceous is dominated by shallow marine facies (Guiraud and Bosworth 1999), while during the Upper Cretaceous, the environment of deposition changed from open-marine to marine-alluvial sediments before returning back to marine conditions as the continental margins of Egypt underwent submergence with the gradual sinking of the Mediterranean at the end of the Cretaceous (Said 1990; Guiraud and Bosworth 1999). Up to the Eocene, this submergence continued with the gradual sinking of the Mediterranean; the late Cretaceous-Eocene deposits are represented by carbonate-dominant sediments intercalated by clastic layers as a result of regional marine transgression, which ended with mega-Syrian arc tectonics (Harms and Wray 1990). During the Oligocene, the ultimate isolation of the Mediterranean basin was caused by the northward accelerated drift of the Arabian Plate, forming a strong uplift, rejuvenating the Syrian arc

uplifts, and resulting in clastic dominant deposition rather than Eocene carbonate dominant deposition. Consequentially, thick shale deposits (Dabba/ Tineh formations) act as source rocks, intercalated with turbidity slope channels, which act as the main reservoir of the Oligocene system. At the Lower Miocene, another regional transgression covered the whole northern part of Egypt and made a connection between the Red and Mediterranean seas, so that deposits of this age (the Qantara Formation) were represented by a thick sequence of basinal marls and shales with subordinate coarse terrigenous influx. During the Middle Miocene, a considerable subsidence rate and a large sediment supply led to the development of a thick terrigenous sequence (the Sidi Salem Formation). At the end of the Serravallian, erosive unconformity was recorded in the area by the unconformity of the Serravallian/Tortonian age (Barber 1981; Harms and Wray 1990; Said 1990), as a result of the sea regression, which was represented by predominated sand and shale deposition (Qawasim / Wakar formations), and in some places the younger layers directly overlaid the Serravallian deposits. During the Late Miocene, Early Messinian, the closure of the Strait of Gibraltar accompanied by isolating the fluvial drainage from the seawater led to Messinian Salinity Crises (MSC), which are represented in the stratigraphical record by a thick evaporites sequence (Rosetta Formation) intercalated in some locations with limestone, dolomitic, clastic sediments, or even totally eroded and diluted in some locations. Overlaid by clastic (Abu Madi Formation) sediments were accumulating within intricate climatic and depositional settings, it's evident that both the depositional and diagenetic facies were undoubtedly influenced. Consequently, this exerted a substantial influence on the reservoir properties of the Abu Madi facies, given the diverse nature of the Abu Madi Formation, encompassing a spectrum from continental (fluvial) to estuarine (deltaic) facies (Salem et al. 2005; Leila et al. 2020). Later on, due to the opening of the Strait of Gibraltar and the reconnection of the Atlantic Ocean with Mediterranean water, MSC has

been ended, which was recorded within the geological column with the second Miocene unconformity (Leila and Moscariello 2019). and the main transgression happened within the Pliocene; thick prograding marine sequences were deposited with a well-developed slope to basal submarine channel complexes (Kafr EL Sheikh Formation) (Gargani and Rigollet 2007). During the Pleistocene and younger, the sea transgression amplitude decreased with a deposition system consisting mainly of shale intercalated with channels of varying reservoir quality sands in varying small and sometimes interconnected traps. Lateral variation is very strong amongst relatively uniform, flat, dirty sand (Gargani and Rigollet 2007).

3 Methodology and dataset

As a multi-approach study, several methods and geological disciplines were used to achieve the study's objectives, these will be discussed below:

3.1 Sequence stratigraphy

The sequence stratigraphy approach was used as a cornerstone in the current work; sequence stratigraphic analyses were guided by models and principles of fluvial / bio-sequence stratigraphy following Catuneanu *et al.*, 2006. borehole logs and calculated curves (e.g., GR and Vsh) integrated with bio-stratigraphical data to define sequence boundaries during its evolution. Litho-chronostratigraphic correlation, which shows thickness variation, may give hints about regions of subsidence and uplift. Sequence stratigraphic models may, however, be used to accurately identify the controls on the temporal and spatial distribution of sediments (Braaksma *et al.* 2006). Sequence stratigraphic analyses divide stratigraphic records into depositional sequences with boundaries marked by subaerial erosion (unconformity) surfaces or their correlative conformities (Mitchum *et al.* 1977). A sequence boundary (erosion surface or temporal equivalent

surface) marks an abrupt basinward shift in the deposition (Posamentier and Vail 1988).

3.2 Reservoir petrophysical evaluation

Electrical logs (E. logs) have been extensively used in a quantitative and qualitative way to determine reservoir lithology and petrophysical characteristics (such as porosity, Vsh and resistivity), fluid pressure, fluid sampling, as well as fluid type, calculation of reserves, and determination of productivity (Asquith, 1982). By using gamma-ray (GR) deep resistivity (Res) and neutron-density (Neu/Den) curves, an evaluation set of petrophysical criteria is delivered to assess the potentiality of Oligocene deposits to act as reservoirs and to determine reservoir quality and attributes (such as shale volume, porosity, and hydrocarbon saturation).

3.3 1D Basin modeling

To generate a 1D model for every single well in the study, variable types of data were integrated with each other to achieve the purpose of this study. Chronological surfaces: where the well data and logs sub-divided into chronologic-based intervals (9 intervals within Salamat-1, 10 intervals within X-1, 10 within Notus1-st2 and 10 within Helm-1st1 wells), lithology and facies associations: where the chronologic-based interval sub-divided according to facies and facies associations, vitrinite reflectance data: averaging the Ro values within every source rock unit (6 and 4 samples within X-1 well, 8 and 3 samples within Salamat-1 well, 14 and 4 samples within Notus1-st2 well and in the last 4 and 3 samples within Helm-1st1 well, for Chattian and Rupelian source rock units respectively), and rock-eval pyrolysis data: averaging the pyrolysis values for every source rock unit were used, (About 72 and 17 samples within Atoll-1st1 well, 70 and 19 samples within Salamat-1 well, 215 and 25 samples within Notus1-st2 well, and in the last 27 and 10 samples within Helm-1st1 well, for Chattian and Rupelian source rock units, respectively).

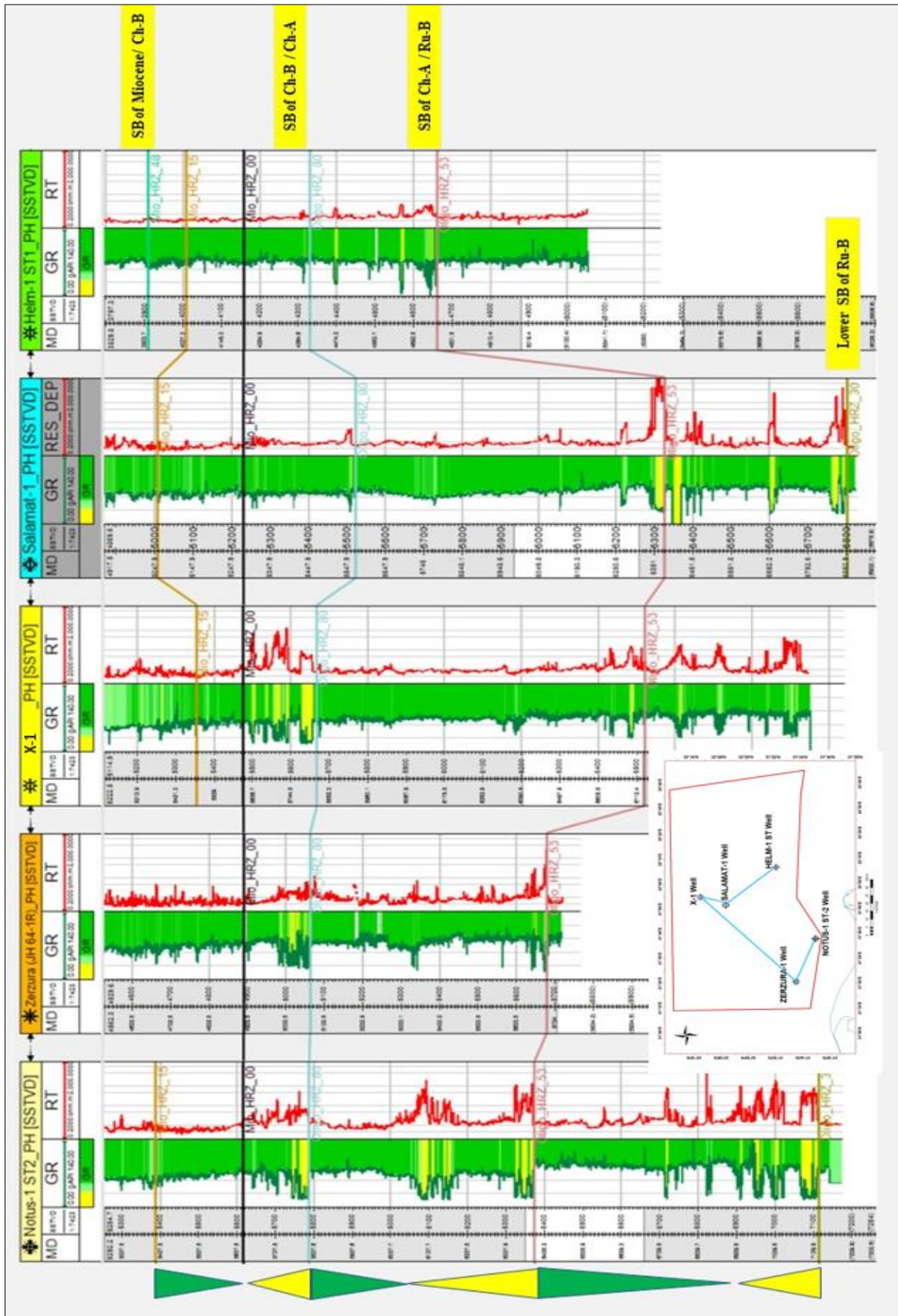


Fig. 2. stratigraphic correlation panel showing Three 3rd order sequence cycles identified within five wells in the study area.

4 Results and discussions

4.1 Sequence Stratigraphy

Sequence stratigraphy workflow (using regional chrono-stratigraphic horizons, litho-stratigraphic concepts and wireline logs) resulted in three 3rd order sequence cycles (two of Chattian age and one of Rupelian age) that aligned with Haq, 1987 3rd order of relative sea level changes, resulted in chrono-stratigraphical correlation along all provided wells. The well log-based sequence correlation (Fig. 2) emphasized changes in relative sea level. A number of three third-order depositional sequences were recognized, formed in a continental slope setting and dominated by Oligo-Miocene deposits. It is built upon lateral and vertical shifts between turbidity channels, slope fans, and basin floor fan facies. Oligo-Miocene sequence stratigraphic subdivision demonstrates the stacking patterns and stratigraphic framework of different lithologies and lithofacies preserved in the area of study and helps define historical stages of change at the base level, which marks the evolution of the studied sequence.

4.2 Reservoir petrophysical Evaluation:

An intensive petrophysical evaluation was conducted for the Lowstand System Tract (LST), where the higher the chance of coarse-grained deposit accumulation (consequently the main occurrence of reservoirs), in five studied wells, eleven LST were determined within three 3rd order sequence stratigraphy cycles within Oligocene deposits. As shown below Table.1.

A total of thirteen 3rd order sequence cycles have been discovered in five studied wells. Among these, ten cycles belong to the Chattian age and are present in Salamat-1, Notus1-st2, X-1, Helm-1st1, and Zorzura-1 wells. The remaining three cycles represent the Rupelian age and can be found in Salamat-1, Notus1-st2, and X-1 wells.

It is important to note that some wells do not contain Rupelian cycles because drilling operations stopped within the Chattian-aged deposits.

Table. 2 provides the petrophysical analysis for the Chattian and Rupelian Reservoirs. The term "gross cycle" refers to the total vertical depth subsea thickness of the entire 3rd order sequence cycle. "Gross LST" represents the total vertical depth subsea thickness of the Lowstand System tract, which corresponds to the thickness of sand within the sequence cycle. "Net sand" indicates the thickness of sand with a shale fraction of no more than 45% of the sand volume (Vsh cutoff). "Net reservoir" represents the thickness of sand with an effective porosity of at least 10% (porosity cutoff). "Net HC bearing reservoir" refers to the thickness of reservoir with a minimum hydrocarbon saturation of 30% of the total fluid saturation within the effective porosity.

Several statistical parameters are included to determine the occurrence and thickness of sand relative to the overall thickness of the Lowstand System tract, the number of reservoirs, and the number of hydrocarbon-bearing reservoirs within the Lowstand System tract. These parameters include "N/G" which displays the ratio of reservoir thickness over net sand thickness the higher ratio of N/G indicates higher percentage of the deposited sand works as reservoir which means good porosity values with no tightness or compaction, "average net reservoir" which represents the average thickness of a reservoir body, "average gross sand" which displays the ratio of reservoir occurrence per Lowstand System tract thickness as a representation of the reservoir occurrence within the LST, and "Average Net/Average Gross" which represents the average net reservoir thickness over the average gross sand thickness. Additionally, two statistical features are provided: the thickness of reservoir and the thickness of hydrocarbon-bearing reservoir per a constant thickness of the sequence cycle (proposed as 500m). These features allow for correlation of the presence and thickness of sand and hydrocarbon-bearing sand across different wells with the same age reservoirs' gross thickness.

Table 1. the 3rd order sequence stratigraphy cycles penetration within five studied wells.

Epoch	Stage	Sequence Cycle	Wells				
Oligocene	Chattian	Ch_B	Salamat-1	Notus-1St2	X-1	Zorzura-1	Helm-1st1
		Ch_A	Salamat-1	Notus-1St2	X-1	Zorzura-1	Helm-1st1
	Rupelian	Ru_B	Salamat-1	Notus-1St2	X-1		

Table 2. petrophysical analysis results for the Chattian and Rupelian Reservoirs (Ch_B, Ch_A and Ru_B sequence cycles) in the studied five wells, offshore Nile Delta.

Well Name	Cycle Name	Cycle interval		Gross Cycle thickness (m)	LST interval		Gross LST(m)	Net Sand (m)	Net Reservoir (m)	Net HC bearing Reservoir (m)	Number of Reservoirs	Number of HC bearing Reservoir	Average Res Vsh (v/v)	Average Res Porosity (v/v)	Average Res Sw (v/v)	N res/G sand	Avg net reservoir (m)	Avg Gross sand (m)	Aver N/Aver G	thick. Res /500	thick. HC bearing Reservoir /500
		from (m)	to (m)		from (m)	to (m)															
HELM-1St1	Ch_B	3979.22	4320	340.78	4150	4320	170	1.644	1.644	0	1	0	0.21	0.19	0.98	1.000	1.64	170.00	0.010	2.4	0.0
Salamat-1		5005	5511	506	5244.316	5511	267	16.526	12.526	0	4	0	0.379	0.129	0.98	0.758	3.13	66.66	0.047	12.4	0.0
X-1		5246	5659	413.384	5490	5659.4	169	76.482	68.715	33	4	3	0.166	0.162	0.684	0.898	17.18	42.35	0.406	83.1	39.9
Zerzura-1		4677.905	5061	383	4900	5060.9	161	43.192	40.309	0	5	0	0.13	0.16	0.98	0.933	8.06	32.20	0.250	52.6	0.0
Notus-1St2		5387	5788	401	5600	5788.2	188	62.764	31.838	0	2	0	0.068	0.138	0.985	0.507	15.92	94.09	0.169	39.7	0.0
HELM-1St1	Ch_A	4320	4650	330.9	4550	4650	100	9.741	8.10	0	2	0	0.14	0.17	0.96	0.832	4.05	50.00	0.081	12.2	0.0
Salamat-1		5510.96	6330	804	5980	6329.8	350	85.663	46.978	27.258	4	2	0.137	0.075	0.252	0.548	11.74	87.45	0.134	29.2	16.9
X-1		5659.384	6500	840.616	6150.605	6500	349	23.668	16.31	0	3	0	0.195	0.144	0.802	0.689	5.44	116.47	0.047	9.7	0.0
Zerzura-1		5060.905	5680	615	5250	5680	430	18.708	17.28	5.6	2	2	0.143	0.14	0.75	0.924	8.64	215.00	0.040	14.0	4.6
Notus-1St2		5788.175	6374	586	6045.898	6374.4	328.461	104.687	55.9	19.7	7	2	0.057	0.118	0.62	0.534	7.99	46.92	0.170	47.7	16.8
Salamat-1	Ru_B	6329.789	6800	475.73	6600	6800.5	200.499	53.215	40.606	0	3	0	0.39	0.09	0.95	0.763	13.54	66.83	0.203	42.7	0.0
X-1		6500	6933	433	6810	6932.9	123	28.724	8.568	0	2	0	0.314	0.13	0.858	0.298	4.28	61.44	0.070	9.9	0.0
Notus-1St2		6374.359	7111	737	6710.75	7111.2	400	145.177	45.999	26.5	4	3	0.026	0.107	0.583	0.317	11.50	100.12	0.115	31.2	18.0

4.2.1 Ch-B 3rd order cycle

The Ch-B 3rd order cycle is equivalent to the Haq *et al.* 1987 TB1.4 3rd order cycle. In this cycle, the total vertical depth subsea thickness increases from south to north, with measurements of 383m and 340m at Zerzura-1 and Helm wells respectively in the south, and 413m and 506m at X-1 and Salamat-1 wells respectively in the north. The Lowstand System tract records the maximum thickness at Salamat-1 well with 267m and the minimum thickness at Zerzura-1 well with 161m, supporting the overall basinward thickness increase of the sequence cycles. Unlike the cycle and Lowstand System tract, the petrophysical criteria displayed in Figure 3 are not chronologically relevant. Petrophysical criteria are influenced by various depositional conditions such as tectonics, turbidity/slope channel behaviour, and sediment supply rate.

In the X-1 well, which is the most northern location, the thickness of net sand is 76.4m, and the thickness of the net reservoir is 68.7m, with N/G 0.89 which considered direct indication of good porosity and absence of tightness. There is a hydrocarbon-bearing reservoir with a thickness of 33m. The average thickness of the net reservoir is 17m, and the ratio of average net reservoir thickness to average gross sand thickness is 40%. Moving 17 km south from X-1, we reach the Salamat-1 well location, which has a net sand thickness of 16.5m and a net reservoir thickness of approximately 12.5m, with N/G 0.75 which considered direct indication of fair sand porosity and absence of tightness. These measurements suggest that the well location was relatively higher during the deposition, as indicated by the lower values for average net reservoir 3m and average net reservoir to average gross sand ratio 4%.

Further southeast, at the Helm-1St1 well location, both net sand and net reservoir thicknesses decrease to

1.6m. The average net reservoir thickness is 1.6m, with N/G 1 considering all the deposited sand effectively works as reservoir. The ratio of average net reservoir thickness to average gross sand thickness is 1%. These results demonstrate an overall thinning of sand and reservoir in the southeastern part of the basin. The location of the Helm-1St1 well was relatively higher than the surrounding area, which explains the observed thinning.

Moving southwest to the Zerzura-1 well, the net sand thickness is 43m, and the net reservoir thickness is 40m, with N/G 0.93 considering almost all the deposited sand effectively works as reservoir. The average net reservoir thickness is 8m, and the ratio of average net reservoir thickness to average gross sand thickness is 25%. Further south, near the shoreline, we find the Notus-1St2 well, which encountered a net sand thickness of 62.7m and a net reservoir thickness of 31.8m, with N/G 0.5 displaying clear sand tightness which decreases the percent of porose sand to half of its original thickness. The average net reservoir thickness is 15.9m, and the ratio of average net reservoir thickness to average gross sand thickness is 16%.

The comparison of reservoir thickness to a constant value allows us to determine whether the reservoir thickness is appropriate, thicker, or thinner relative to the overall thickness of the cycle. The reservoir thickness per 500m varies widely within the studied wells. For example, in the Helm-1St1 well, it is only 2.4, which is insignificant compared to the more basinward Atoll1-St1 well with a value of 83, indicating a trend of reservoir thickening basinward and thinning towards the southeast. In contrast, the Zerzura-1 and Notus-1St2 wells in the southwest show less thinning with values of 52.6 and 39.7, respectively.

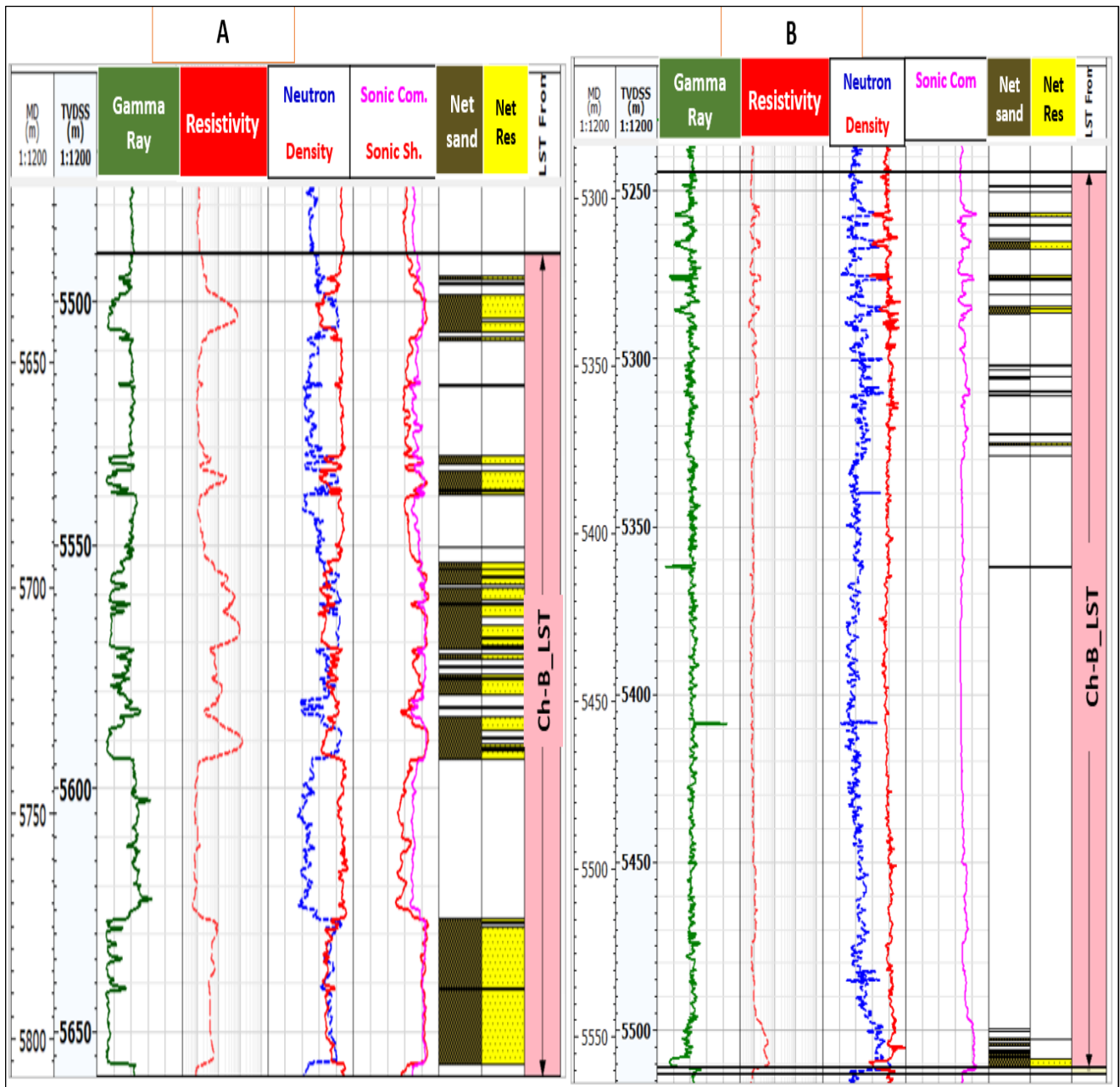


Fig. 3a. Ch-B_LST CPI showing Gross LST, Net Reservoir and Net Sand distribution within (A) X-1 and (B) Salamat-1 wells.

The effective porosity values exhibit a wide range, with the maximum value of 19% observed at the shallowest occurrence of the Ch-B 3rd order cycle in the Helm-1st1 well. The porosity then decreases to 16% at both the X-1 and Zerzura-1 wells, further decreasing to 13% at the Notus-1St2 well, and finally

reaching 12% at the deepest occurrence of the Ch-B 3rd order cycle in the Salamat-1 well. The correlation of porosity values within the studied wells highlights the significant influence of overburden thickness on porosity.

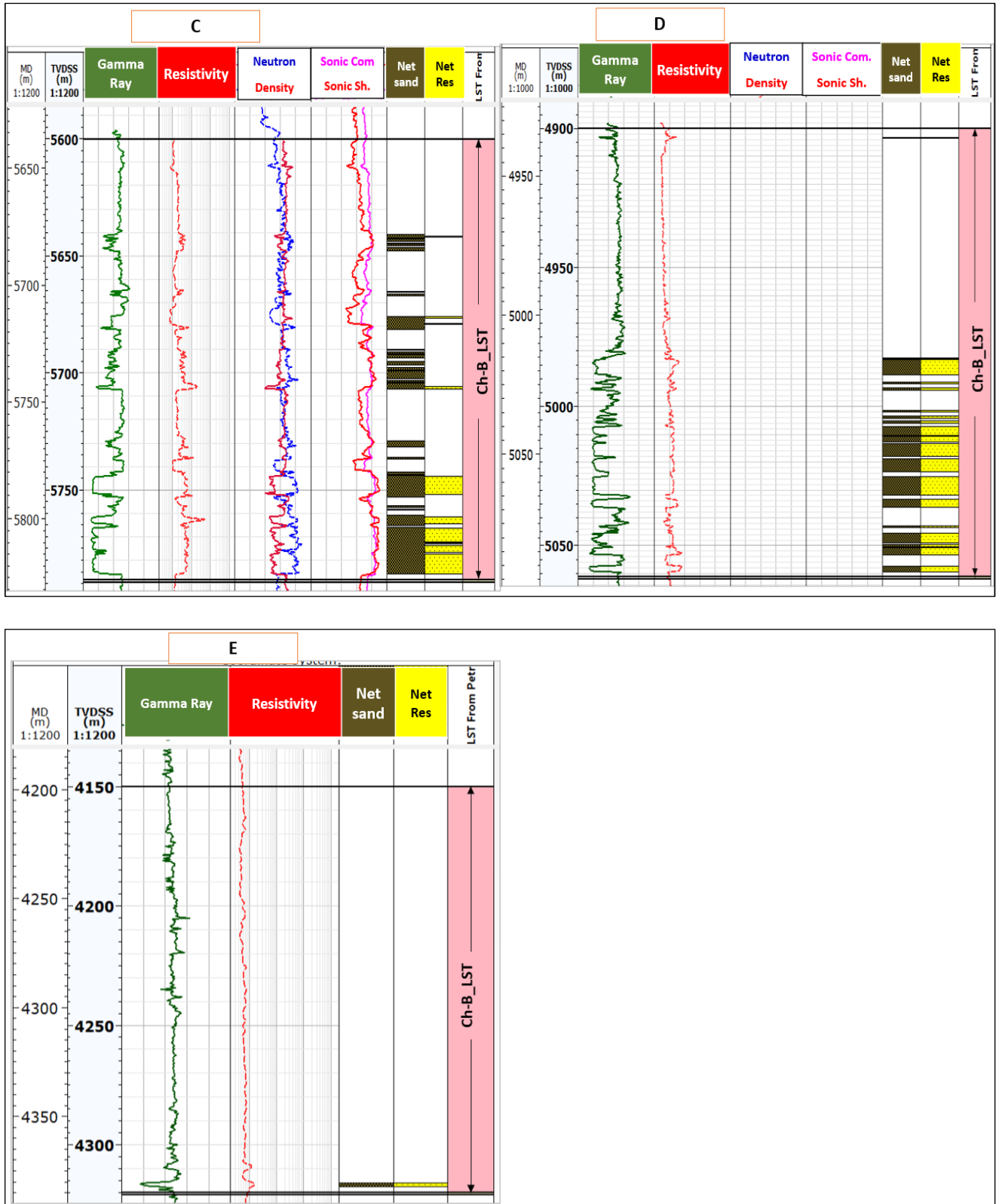


Fig. 3b. Ch-B_LST CPI showing Gross LST, Net Reservoir and Net Sand distribution within (C) Notus-1St2, (D) Zerzura-1 and (E) Helm-1st1 wells.

4.2.2 Ch-A 3rd order cycle

The Ch-A 3rd order cycle, which is equivalent to the Haq et al. 1987 TB1.3 3rd order cycle, displays variations in true vertical depth subsea thickness across different well locations. Starting from the southeast, the Helm well location records a thickness of 383m for the entire cycle. Moving north, the maximum thickness is observed at the X-1 and Salamat-1 wells, with measurements of 840m and 804m, respectively. On the other hand, in the southwest, the thickness decreases to 615m and 586m in the Zorzura-1 and Notus-1St1 wells, respectively.

In terms of the Lowstand System tract (LST) thickness, the Helm well location records a thickness of 100m. This thickness increases to 350m in both the Salamat-1 and X-1 wells located in the north. In the southwest, the thickness decreases to 328m in the Notus-1St2 well, while the Zorzura-1 well has a thickness of 430m.

Examining the petrophysical criteria presented in Fig. 4, the X-1 well exhibits a net sand thickness of 23.6m and a net reservoir thickness of 16.3m, with N/G 0.69 indicating the percentage of deposited sand effectively works as reservoir. The average net reservoir thickness is 5.4m, and the ratio of average net reservoir thickness to average gross sand thickness is 4.7%. At the Salamat-1 well location, the net sand thickness is 85m, and the net reservoir thickness is approximately 47m, indicating relatively thicker formations compared to the X-1 location, lower N/G 0.55 considering almost half of the deposited sand effectively works as reservoir. The average net reservoir thickness is 11.7m, and the ratio of average net reservoir thickness to average gross sand thickness is 13.4%.

Moving southeast to the Helm-1St1 well location, both the net sand thickness and net reservoir thickness decrease to 9.7m and 8m, respectively, with 0.82 N/G of sands works effectively as reservoir. However, the average net reservoir thickness increases to 4m, and the ratio of average net reservoir thickness to average gross sand thickness is 8%. These results indicate an

overall increase in sand and reservoir thicknesses compared to the Ch-B 3rd order cycle sand and reservoir thicknesses in the same well location. Nevertheless, there is still a general thinning observed in the southeastern part of the basin when compared to sand and reservoir thicknesses in other wells.

To the southwest, the Zorzura-1 well encountered a net sand thickness of 18.7m and a net reservoir thickness of 17.2m, with N/G 0.91 considering almost all the deposited sand effectively works as reservoir. The average net reservoir thickness was 8.6m, and the ratio of average net reservoir thickness to average gross sand thickness was 4%.

Moving further south, the Notus-1St2 well displayed thicker sand and reservoir occurrences, with a net sand thickness of 104m and a net reservoir thickness of 56m, with N/G 0.51 showing clear tightness within the sand deposits. The average net reservoir thickness was 7.9m, and the ratio of average net reservoir thickness to average gross sand thickness was 17%.

By determining reservoir thickness per 500m within the studied wells, we can gain a general understanding of the rate of sand deposition. In the Helm-1St1 well, the reservoir thickness reached 12.2 (thicker than the more basinward X-1 well, which measured 9.7). In the Salamat-1 well, the reservoir thickness reached 29.2 (with a 16.9 ratio of hydrocarbon-bearing reservoir thickness per 500m), supporting the trend of reservoir thickening basinward and thinning southeast. To the southwest, there was less thinning observed in the Zorzura-1 well with a ratio of 4.6 hydrocarbon-bearing reservoir thickness per 500m, and surprisingly, the Notus-1St2 well reached 47.7 (with a 16.8 ratio of hydrocarbon-bearing reservoir thickness per 500m).

Effective porosity displayed a wide range of values, with a maximum of 17% at the Helm-1st1 well (the shallowest occurrence of the Ch-A 3rd order cycle) and a minimum of 7% at the Salamat-1 well (the deepest occurrence of the Ch-A 3rd order cycle), influenced by the thickness of the overburden.

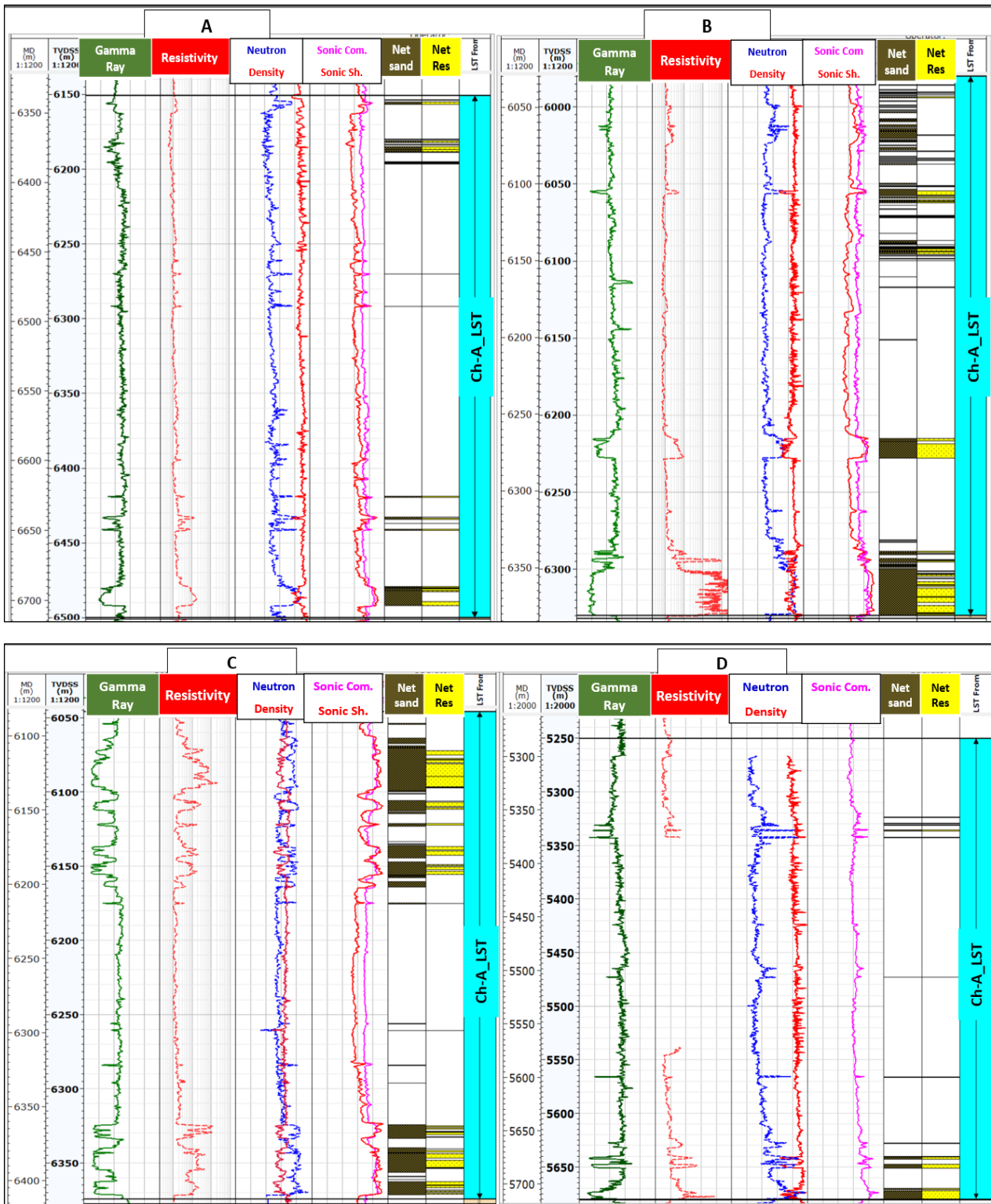


Fig. 4a. Ch-A_LST CPI showing Gross LST, Net Reservoir and Net Sand distribution within (A) X-1, (B) Salamat-1, (C) Notus-1St2 and (D) Zerzura-1 wells.

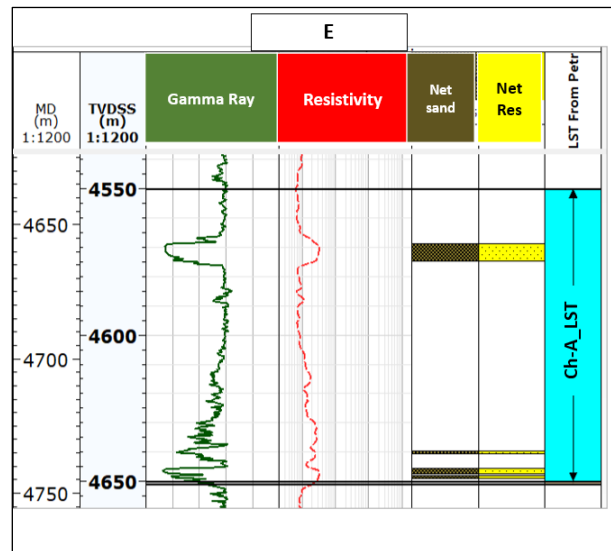


Fig. 4b. Ch-A_LST CPI showing Gross LST, Net Reservoir and Net Sand distribution within (E) Helm-1st1 well.

4.2.3 Rup-B 3rd order cycle

The Rup-B 3rd order cycle, which is equivalent to the Haq et al. 1987 TB1.2 3rd order cycle, was penetrated by only three of the studied wells. The Notus-1St2 well recorded the maximum thickness of 737m, while the thickness decreased from north to basinward, reaching 475m and 433m within the Salamat-1 and X-1 wells, respectively (X-1 well did not show litho-chronostratigraphic proves to be reached the lower sequence boundary of the cycle). The Lowstand System tract (LST) thickness recorded its maximum at the Notus-1St2 well with 400m, which decreased basinward to 200m and 123m in the north at the Salamat-1 and X-1 wells, respectively.

Analyzing the petrophysical criteria for the Rup-B 3rd order cycle in Fig. 5, the Notus-1St2 well displayed a net sand thickness of 145m and a net reservoir thickness of 46m, with N/G 0.31 showing clear tightness within the sand deposits, and an average net reservoir thickness of 11.5m and a ratio of average net reservoir thickness to average gross sand thickness of 11.5%. Moving northward, towards the more basinward X-1 well, the net sand thickness was 28.7m and the net reservoir thickness was 8.5m, with N/G 0.29 showing clear tightness with thick overburden rock, and an average net reservoir thickness of 4.3m and a ratio of average net reservoir thickness to average gross sand thickness of 7%. At the Salamat-1 well location, the net sand thickness was 53m, and the net reservoir thickness was approximately 40m, which were thicker compared to the X-1 location, with N/G 0.75 considering most of the sand effectively works as reservoir. The average net reservoir thickness was

13.5m, and the ratio of average net reservoir thickness to average gross sand thickness is 20%.

Reservoir thickness per 500m for the Rup-B 3rd order cycle in the Notus-1St2 well was determined to be 31m (with approximately 18m representing the thickness of the hydrocarbon-bearing reservoir within that interval). Moving to the more basinward X-1 well, the reservoir thickness per 500m measured 9.9m. In the Salamat-1 well, it reached a value of 42.7. The effective porosity ranges from its maximum value of 13% at the X-1 well, decreases to 10% at the Notus-1St2 well and reaches a minimum of 9% at the Salamat-1 well, which represents the deepest occurrence of the Rup-B 3rd order cycle. These cycles do not influence the porosity trend with respect to overburden thickness. It is interesting to note that the Salamat-1 well is the shallowest, while the X-1 well is the deepest, which highlights the significance of sandstone quality as one of controlling factors.

Petrophysical evaluation result analysis

The **Notus-1St2 well** exhibits low N/G indicating tightness across all stratigraphic cycles, attributed to the maximum overburden thickness observed at this location. The substantial overburden has likely caused intense compaction, reducing porosity and permeability.

In contrast, the **X-1 well** displays a relatively high N/G, indicative of favorable reservoir quality, except in the lower part, where a thick overburden reduces its effectiveness.

The **Salamat-1 well** shows higher net-to-gross (N/G) ratios compared to the other wells. This can be attributed to the position of the Salamat ridge, a paleo-high that experienced reduced overburden, compaction, and subsequent tightness. As a result, the underlying sands maintain better reservoir quality.

Despite this favorable setting, the average sand thickness is limited, suggesting challenges in the deposition of slope channel sands across the elevated structures.

The **Helm-1st1 well** has the highest N/G values, situated on an elevated Cretaceous structure characterized by minimal overburden and compaction.

Finally, the **Zerzura-1 well**, also influenced by a paleo-elevated structure, shows good N/G values across the two studied cycles and maintains a fair gross sand thickness. The reduced overburden has likely preserved better reservoir properties.

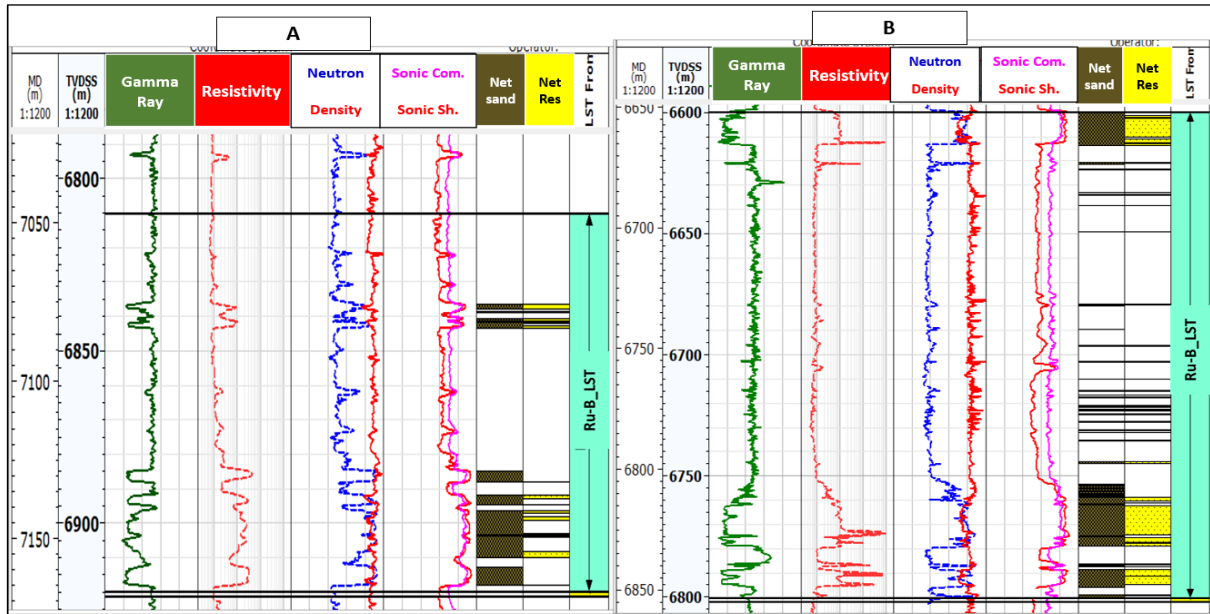


Fig. 5a. Ru-B_LST CPI showing Gross LST, Net Reservoir and Net Sand distribution within (A) X-1 and (B) Salamat-1 wells.

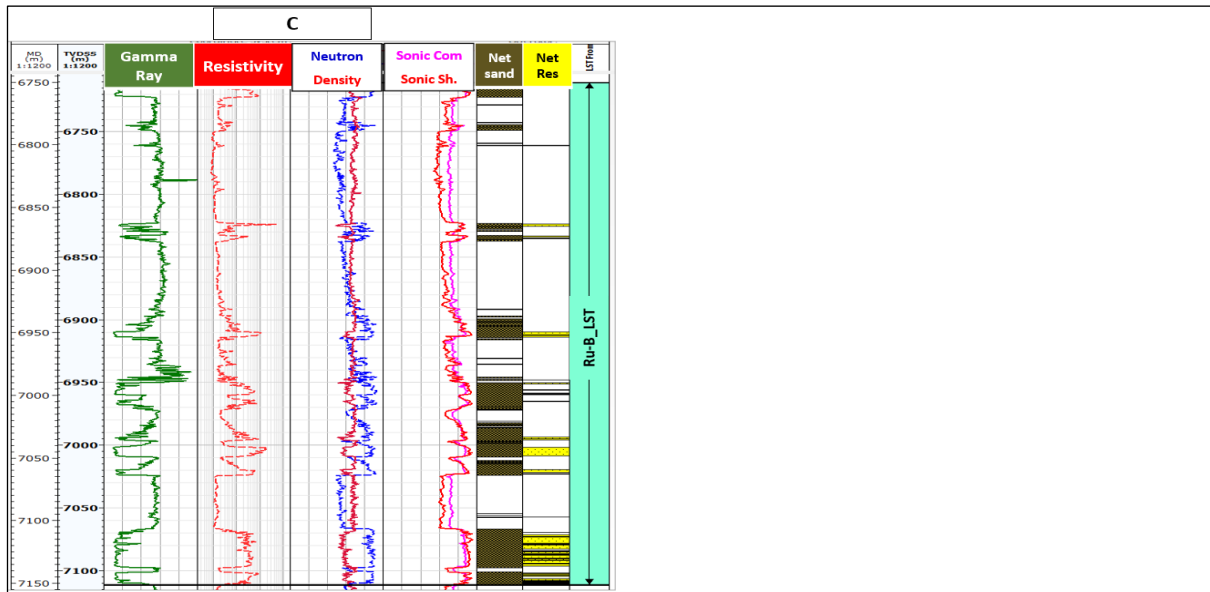


Fig. 5a. Ru-B_LST CPI showing Gross LST, Net Reservoir and Net Sand distribution within (C) Notus-1st2 well.

4.3 1D Basin Modeling

Both the thermogenic and biogenic hydrocarbon sources have been identified in the known Nile Delta and Mediterranean petroleum systems. In Cretaceous, Eocene, Oligocene, and Late Miocene rock formations, thermogenic sources proved as predominantly hydrocarbon feeders, with less contribution from biogenic sources. In contrast, none of the Middle, Late Miocene, or younger deposits have proven to be mature source rocks. Therefore, the biogenic source rock is the sole active source, unless a deep-seated fault acts as a migration pathway, delivering thermogenic hydrocarbons to the younger layers. An intensive 1D basin modelling workflow has been carried out to determine the thermal maturation of source Oligo-Miocene in this study. An extended

dataset has been used including chrono-stratigraphical data, litho-stratigraphical data, total organic carbon (TOC), rock-eval pyrolysis data, and kinetics data. Four wells were selected strategically across the basin to serve as control points. The primary objective of the 1D basin modeling was to identify the depths and timing of hydrocarbon generation and expulsion for the Oligocene-aged source rock. To improve the accuracy of the model and reduce uncertainties, it was crucial to incorporate appropriate boundary conditions such as heat flow, subsurface water influx, and paleo-water depth. The Oligocene interval source rock was subdivided based on its deposition age into three units: **Ch_B**, **Ch_A**, and **Ru-B**.

Table 3. 1D basin modeling results for Chattian and Rupelian deposits (Ch_B, Ch_A and Ru_B source rock units) in the studied four wells, offshore Nile Delta.

Well Name	source rock unit	Sub-unit	Time Span		Lithology	thickness m	TOC %	HI mgHC/gTOC	Critical Moment Ma	Peak of Generation rate mgHC/gTOC/Ma	Total Generated Mass Mton
			From (Ma)	To (Ma)							
HELM-1St1	Ch_B	-	26.29	23.03	100 Shale	158	1.1	41.2	0.64	No peak	un determinable
Salamat-1					80sh10si10sa	388	1.16	115	1.1	6.00	0.04
X-1					30sh70sa	256	1.07	180	1.98	11.8	0.08
Notus-1St2					70sh30sa	191	1.06	185.7	11.4	18.00	0.2
HELM-1St1	Ch_A	-	27.82	26.29	60sh40sa	376	1.05	35.8	0.98	No peak	un determinable
Salamat-1		Ch_A_3			274	1.2	130	3.31	9.85	0.06	
		Ch_A_2			274			6.3	16.4	0.1	
		Ch_A_1			275			8.79	19.9	0.16	
X-1		Ch_A_3			301	1.1	194	4.91	12	0.17	
		Ch_A_2			302			6.7	17.9	0.27	
		Ch_A_1			302			8.9	24.3	0.38	
Notus-1St2		Ch_A_2			295	1.25	150	11.43	16.75	0.48	
		Ch_A_1			294			11.85	8.64	0.55	
HELM-1St1		Ru_B			Ru_B_2	30.64	27.82	80sh20sa	232	1.1	65.8
Salamat-1	Ru_B_1		233	1.72	No peak			0.01			
	Ru_B_2		250	1.14	129			10.34	22.4	0.18	
X-1	Ru_B_1		250					11.23	28.6	0.24	
Notus-1St2	Ru_B_2		246	0.82	147			10.27	23.5	0.23	
	Ru_B_1		246					11.19	26.4	0.29	
	Ru_B_2		395	1.2	123.4			12.5	7	0.66	
Ru_B_1	395		15.54					12.4	0.74		

This subdivision was carried out using a sequence stratigraphy approach that had previously been employed in reservoir petrophysical evaluation. To assess the effectiveness and potential of each source rock unit, three curves were calculated for each unit within the studied wells. The Vitrinite Reflectance Ro (EASY% Ro Model Sweeney JJ, Burnham AK., 1990) is represented by a solid curve, the Generation rate (GR) is represented by a pointed curve, and the

Generation mass (GM) is represented by a dashed curve (Fig.s 6-11).

The Ch_B source rock, which constitutes the uppermost source rock unit in the area under investigation, corresponds to the upper Chattian deposits, dating from approximately 23.03 Ma to 26.29 Ma. It primarily comprises shale deposits, transitioning from 100% shale content at Helm-1st1

well to gradually diminishing levels of 80% shale at Salamat-1 well, 70% shale at Notus-1st2 well, and reaching its thinnest point 30% shale content at X-1 well (see Table 3). Interestingly, in certain wells, the Ch_B source rock also serves as a reservoir rock due to the substantial presence of thick sand layers in its upper section.

The total organic carbon (TOC) content in this source rock shows considerable variation, ranging from 1.16% at Salamat-1 well, decreasing to 1.1% at Helm-1st1 well, down to 1.07% at X-1 well and reaching its lowest at 1.06% at Notus-1st2 well (see Table 3). The Hydrogen Index (HI), which quantifies the amount of hydrogen relative to the organic carbon content, tends to increase as the source rock matures. HI values range from 185 to 180 mgHC/gTOC at Notus-1st2 well and X-1 well, respectively, decreasing to 115 mgHC/gTOC at Salamat-1 well and reaching a minimum of 41.2 mgHC/gTOC at Helm-1st1 well (Table 3).

Among the studied wells, the Ch_B source rock at Notus-1st2 exhibits the highest total hydrocarbon generation, amounting to 0.2 million tons, as it experienced its critical moment earliest at 11.4 Ma and reached the highest peak generation rate at 18 mgHC/gTOC/Ma. X-1 well ranks as the second-largest generator with a total mass of 0.08 million tons and the second-highest peak generation rate of 11.8 mgHC/gTOC/Ma, but it had a much younger critical moment at 1.98 Ma. In contrast, Salamat-1 well shows less mature source rock, producing a total mass of 0.04 million tons, with a critical moment at 1.1 Ma and a lower peak generation rate of 6.00 mgHC/gTOC/Ma. Finally, Helm-1st1 well, representing the least mature source rock within the Ch_B source rock unit, exhibits virtually undetectable hydrocarbon generation mass, characterized by a flat generation rate curve and relatively recent critical moment occurring at 0.64 Ma (Fig. 6).

The Ch_A source rock, which constitutes the middle regional source rock unit in the area of study, represents sedimentary deposits from the lower Chattian period, spanning approximately 26.29 Ma to 27.82 Ma. It primarily consists of shale deposits, with shale content ranging from 80% at the X-1 and Notus-1st2 wells, gradually decreasing to 60% at the Salamat-1 and Helm-1st1 wells (Table 3).

The average total organic carbon (TOC) content exhibits significant variation, ranging from 1.25% at

the Notus-1st2 well, decreasing to 1.2% at the Salamat-1 well, down to 1.1% at X-1 well and reaching a minimum of 1.05% at the Helm-1st1 well (Table 3). Hydrogen Index (HI) values vary from a maximum of 194 mgHC/gTOC at the X-1 well, decreasing to 150 mgHC/gTOC at the Notus-1st2 well, further reducing to 130 mgHC/gTOC at the Salamat-1 well, and reaching a minimum of 35.8 mgHC/gTOC at the Helm-1st1 well (Table 3).

Due to its considerable thickness, the Ch_A source rock unit has been subdivided into stacked thinner subunits to more accurately model the critical moment, peak generation rate, and total hydrocarbon generation. Three source rock subunits have been identified within the Salamat-1 and X-1 wells, while two are found within the Notus-1st2 well.

Within the X-1 well, three subunits have been identified from younger to older: Ch_A_3, Ch_A_2, and Ch_A_1. The less mature Ch_A_3 subunit has produced a total of 0.17 million tons of hydrocarbon, with a critical moment at 4.9 Ma and the lowest peak generation rate among the three subunits at 12 mgHC/gTOC/Ma. The second subunit, Ch_A_2, has generated a total mass of 0.27 million tons, with a critical moment at 6.7 Ma and a peak generation rate of 17.9 mgHC/gTOC/Ma. The oldest and most mature source rock unit, Ch_A_1, has yielded 0.38 million tons of hydrocarbon, with a critical moment at 8.9 Ma and a peak generation rate of 24.3 mgHC/gTOC/Ma (Fig. 7).

In the Salamat-1 well, three subunits have also been identified, again from younger to older: Ch_A_3, Ch_A_2, and Ch_A_1. The less mature Ch_A_3 subunit has generated 0.06 million tons of hydrocarbon, with a critical moment at 3.31 Ma and the lowest peak generation rate among the three subunits at 9.85 mgHC/gTOC/Ma. The second subunit, Ch_A_2, has produced 0.1 million tons of hydrocarbon, with a critical moment at 6.3 Ma and a peak generation rate of 16.4 mgHC/gTOC/Ma. The oldest and most mature source rock unit, Ch_A_1, has yielded 0.16 million tons of hydrocarbon, with a critical moment at 8.79 Ma and a peak generation rate of 19.9 mgHC/gTOC/Ma (Fig. 8).

Within the Notus-1st2 well, two subunits have been identified from younger to older: Ch_A_2 and Ch_A_1. The less mature Ch_A_2 subunit has generated 0.48 million tons of hydrocarbon, with a

critical moment at 11.43 Ma and a peak generation rate of 16.75 mgHC/gTOC/Ma. The oldest and most mature source rock unit, Ch_A_1, has produced 0.55 million tons of hydrocarbon, with a critical moment at 11.85 Ma and a peak generation rate of 8.64 mgHC/gTOC/Ma (Fig. 9).

Finally, in the Helm-1st1 well, the Ch_A source rock unit is marginally mature, with a relatively recent critical moment at 0.98 Ma. It exhibits a flat generation rate curve, and the generated hydrocarbon mass is too minimal to be detected (Fig. 9).

Among the examined wells, Notus-1st2's Ch_A source rock stands out as the highest contributor to total hydrocarbon generation (aggregating the three subunits) at 1.03 million tons. This is notable because it underwent its earliest critical moment compared to all other wells, occurring in the range of 11.85-11.43 million years ago, even though it ranks third in terms of peak generation rate at 16.75 mgHC/gTOC/Ma. In the case of X-1 well, it ranks as the second-largest generator with a cumulative mass of 0.82 million tons, but it experienced a considerably younger critical moment within the range of 8.9 – 4.9 million years ago and boasts the highest peak generation rate at 24.3 mgHC/gTOC/Ma. On the contrary, Salamat-1 well displays less mature source rock, yielding a cumulative total of 0.32 million tons of hydrocarbon, with a critical moment range of 8.7–3.3 million years ago and the second-highest peak generation rate of 19.9 mgHC/gTOC/Ma. Lastly, Helm-1st1 well, representing the least mature source rock within the Ch_B source rock unit, exhibits nearly undetectable hydrocarbon generation mass. Its relatively recent critical moment (in terms of geological age) occurred at 0.98 million years ago.

Ru_B source rock unit, which constitutes oldest regional source rock unit in the studied area examined region, represents sedimentary deposits from the upper Rupelian, spanning from around 27.82 Ma to 30.64 Ma. It predominantly comprises shale deposits, with shale content ranging from 80% at the X-1 and Helm-1st1 wells, gradually decreasing to 60% at the Salamat-1 well, and reaching its lowest occurrence of 50% shale content at the Notus-1st2 location (Table 3). Remarkably, in specific wells, the Ru_B source rock also serves as a reservoir rock, owing to the noteworthy presence of thick sand layers in its lower section (Table 3).

The total organic carbon (TOC) content varies from good to fair, with good levels observed at 1.2% in the Notus-1st2 well, declining to 1.14% at the Salamat-1 well, and further decreasing to 1.1% at the Helm-1st1 well. Fair TOC content of 0.82% is noted at the X-1 well location (Table 3). Hydrogen Index (HI) values range from a maximum of 147 mgHC/gTOC at the X-1 well, decreasing to 129 mgHC/gTOC at the Salamat-1 well, then to 123 mgHC/gTOC at the Notus-1st2 well, and reaching a minimum of 65 mgHC/gTOC at the Helm-1 well (Table 3).

Due to its substantial thickness, the Ru_B source rock unit has been subdivided into stacked thinner subunits to more precisely model the critical moment, peak generation rate, and total hydrocarbon generation. Two source rock subunits have been identified within the X-1, Salamat-1, Notus-1st2, and Helm-1st1 wells. Within the X-1 well, two subunits have been identified from younger to older: Ru_B_2 and Ru_B_1. The less mature Ru_B_2 subunit has generated a total of 0.23 million tons of hydrocarbon, with a critical moment at 10.27 Ma and the lowest peak generation rate among the two subunits at 23.5 mgHC/gTOC/Ma. The oldest and most mature source rock unit, Ru_B_1, has produced 0.29 million tons of hydrocarbon, with an earliest critical moment at 11.19 Ma and a peak generation rate of 26.4 mgHC/gTOC/Ma (Fig. 10).

In the Salamat-1 well, two subunits have also been identified from younger to older: Ru_B_2 and Ru_B_1. The less mature Ru_B_2 subunit has generated a total mass of 0.18 million tons of hydrocarbon, with a critical moment at 10.34 Ma and the lowest peak generation rate among the two subunits at 22.4 mgHC/gTOC/Ma. The oldest and most mature source rock unit, Ru_B_1, has yielded 0.24 million tons of hydrocarbon, with an earliest critical moment at 11.23 Ma and a peak generation rate of 28.6 mgHC/gTOC/Ma (Fig. 10).

Within the Notus-1st2 well, two subunits have been identified from younger to older: Ru_B_2 and Ru_B_1. The less mature Ru_B_2 subunit has generated a total mass of 0.66 million tons of hydrocarbon, with a critical moment at 12.5 Ma and a peak generation rate of 7 mgHC/gTOC/Ma. The oldest and most mature source rock unit, Ru_B_1, has produced 0.74 million tons of hydrocarbon, with an earliest critical moment at 15.54 Ma and a peak generation rate of 12.4 mgHC/gTOC/Ma (Fig. 11).

Within the Helm-1st1 well, two subunits have been identified from younger to older: Ru_B_2 and Ru_B_1. Both units exhibit an early maturation stage. The younger Ru_B_2 subunit has generated a total mass of 0.005 million tons of hydrocarbon, with a critical moment at 1.46 Ma and a flat generation rate curve. The oldest source rock subunit, Ru_B_1, has produced 0.01 million tons of hydrocarbon, with a critical moment at 1.72 Ma and a flat generation rate curve (Fig. 11).

In the context of the investigated wells, the Ru_B source rock found at Notus-1st2 stands out as the highest producer of total hydrocarbons, accumulating a substantial 1.4 million tons. This is notable because it experienced its earliest critical moment, ranging from 15.54 to 12.5 million years ago, surpassing all other wells in terms of the timing of hydrocarbon generation, even though it ranks third in terms of the peak generation rate at 16.75 mgHC/gTOC/Ma.

The X-1 well follows as the second-largest hydrocarbon generator, accumulating a cumulative mass of 0.82 million tons. It is distinct for having a much younger critical moment, spanning from 8.9 to 4.9 million years ago, and boasts the highest peak generation rate of 24.3 mgHC/gTOC/Ma.

In contrast, the Salamat-1 well displays a less mature source rock, contributing a total cumulative mass of 0.32 million tons. Its critical moment ranges from 8.7 to 3.3 million years ago, and it possesses the second-highest peak generation rate at 19.9 mgHC/gTOC/Ma. Finally, the Helm-1st1 well, representing the least mature source rock within the Ch_B source rock unit, exhibits virtually undetectable hydrocarbon generation mass. It is characterized by a flat generation rate curve and features a relatively recent critical moment occurring at 0.98 million years ago.

Basin Modeling result analysis

- Notus-1st2 emerges as the most prospective location, with significant cumulative hydrocarbon generation across all source rock units. Its early and prolonged generation phases enhance the likelihood of effective migration and accumulation.
- The X-1 well, despite younger critical moments, shows strong generation potential with peak rates, indicating active migration and potential for current hydrocarbon accumulations.
- The Salamat-1 well has moderate potential, constrained by later maturation and lower

cumulative generation. However, its reduced compaction may favor better reservoir quality.

- The Helm-1st1 well, with limited hydrocarbon generation across all units, is the least prospective for exploration.

Comparing the present findings with the other worldwide case studies:

Two case studies of 1D Basin Modeling for analogues deltaic basins summarized to compare the results with current study showed as follows:

1. **Mahakam Delta, Indonesia** (Hakimi et al., 2021).

The study used 1D modeling to analyze the maturation and hydrocarbon potential of Miocene source rocks in the Mahakam Delta. Results suggest high gas generation potential, with thermogenic gas expulsion beginning at 10 Ma and peaking around 8 Ma.

- TOC Content: 1.5% – 5.0%
- Critical Moment: 10 Ma
- Peak Generation: 8 Ma
- Expected Hydrocarbon Generation: 0.5- 2 million tons (mtons).

2. **Thermal Evolution and Petroleum System Analysis of the Western Black Sea Basin** (Sachsenhofer et al., 2018).

This study applied 1D basin modeling to evaluate the thermal maturity and petroleum system evolution of the Western Black Sea Basin. Results indicated that Upper Cretaceous and Paleocene shales exhibit high hydrocarbon generation potential, with peak generation occurring between 10 and 14 Ma.

- TOC Content: 1.0% – 4.0%
- Critical Moment: 14 Ma
- Peak Generation: 10 Ma
- Expected Hydrocarbon Generation: 0.4 – 3.0 million tons (mtons).

By analyzing the results of these two analogues a conclusion could be resulted that:

1. The TOC content of Nile Delta Basin within the world-wide range of successful petroleum systems.
2. Critical moment and peak generation moment are function of wide range of reasons, among them the depositional age of source rock unit and the maturation degree.
3. The Nile Delta Basin has high hydrocarbon generation potentiality comparing to the analogues case studies.

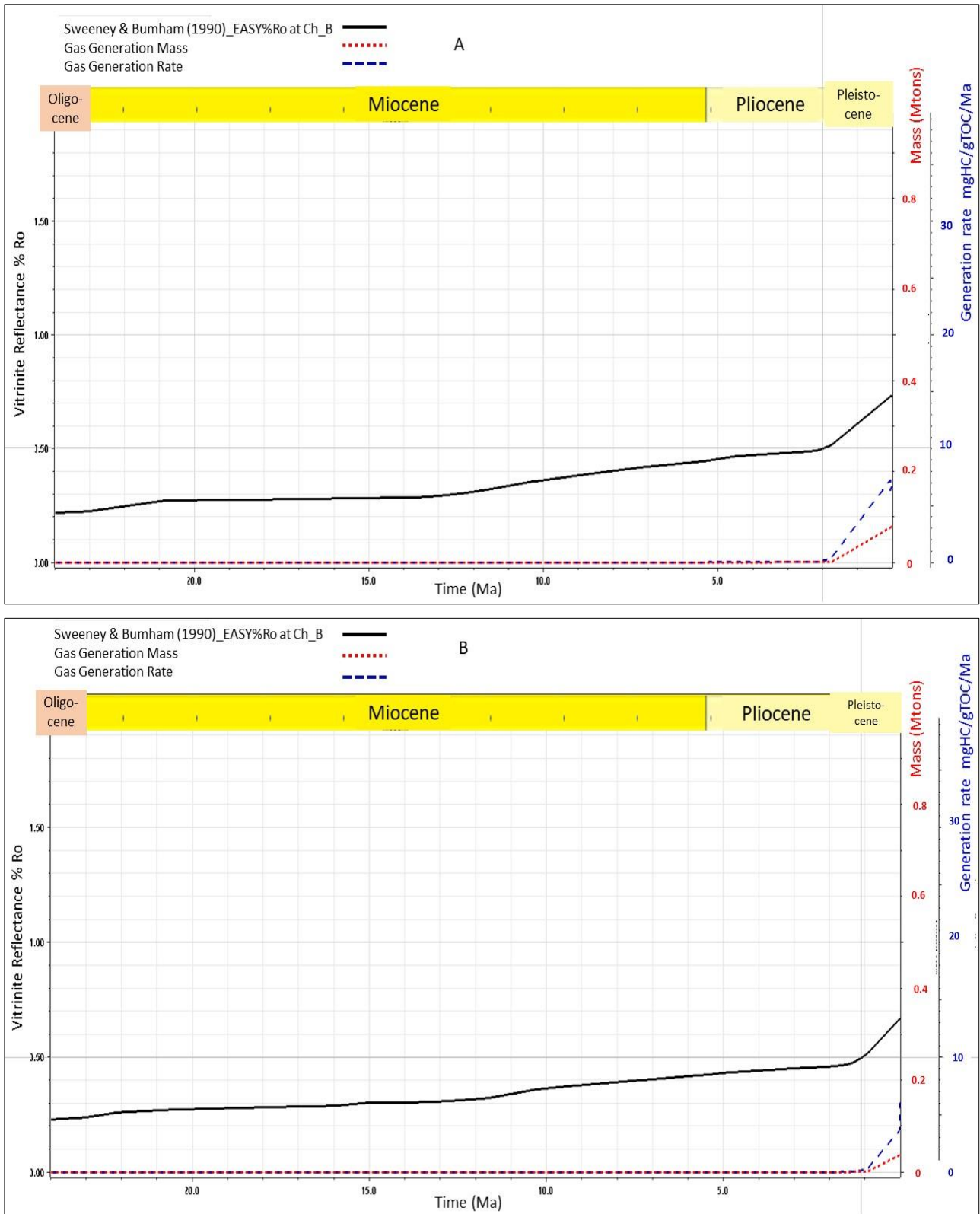


Fig. 6a. Ch_B source rock unit modeling, three curves identified Ro (solid curve), Generation Rate (dashed curve), and Generation Mass (pointed curve). within four wells (A) X-1 well and (B) Salamat-1 well.

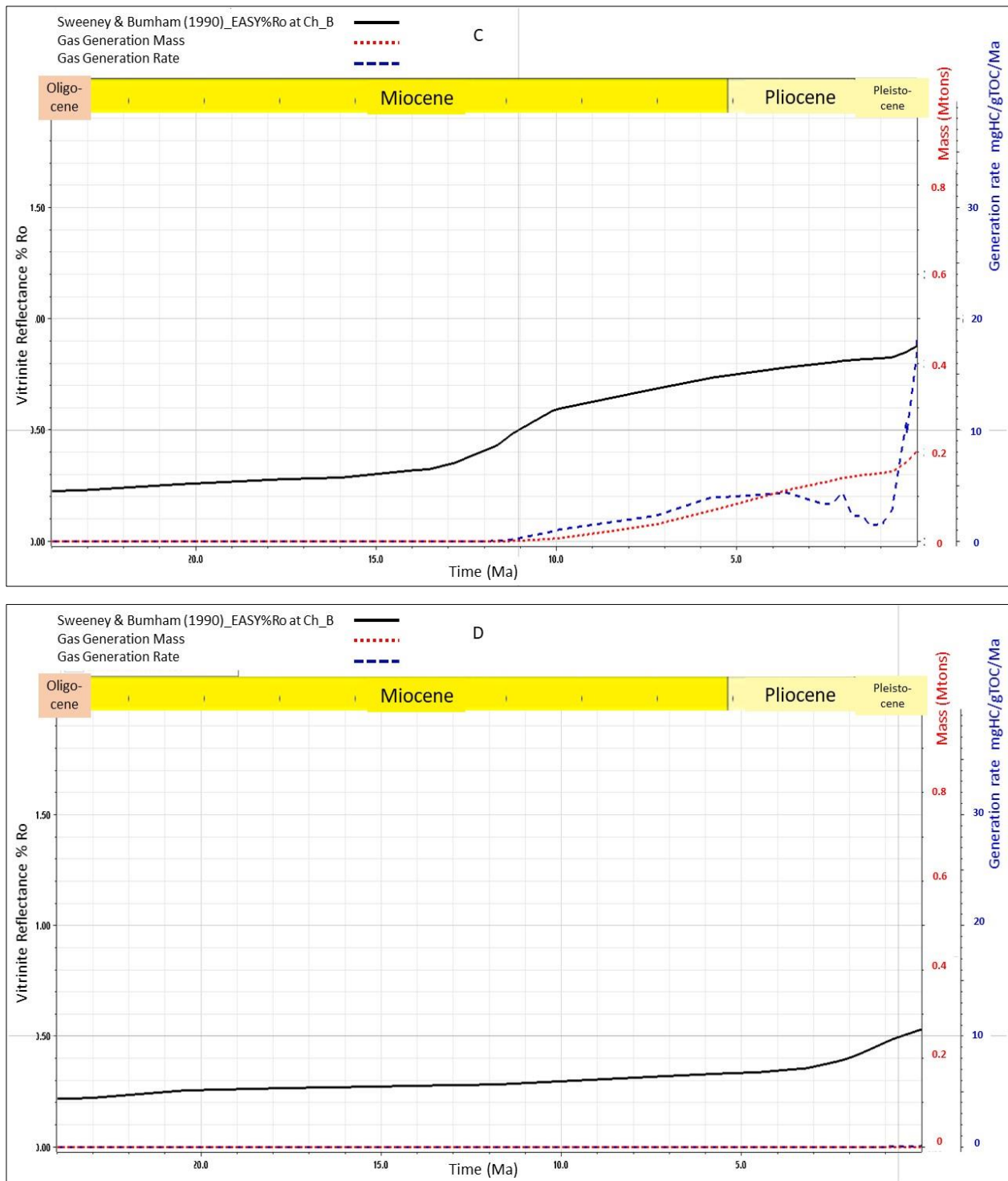


Fig. 6b. Ch_B source rock unit modeling, three curves identified Ro (solid curve), Generation Rate (dashed curve), and Generation Mass (pointed curve), within four wells (C) Notus-1st2 well and (D) Helm-1st1 well.

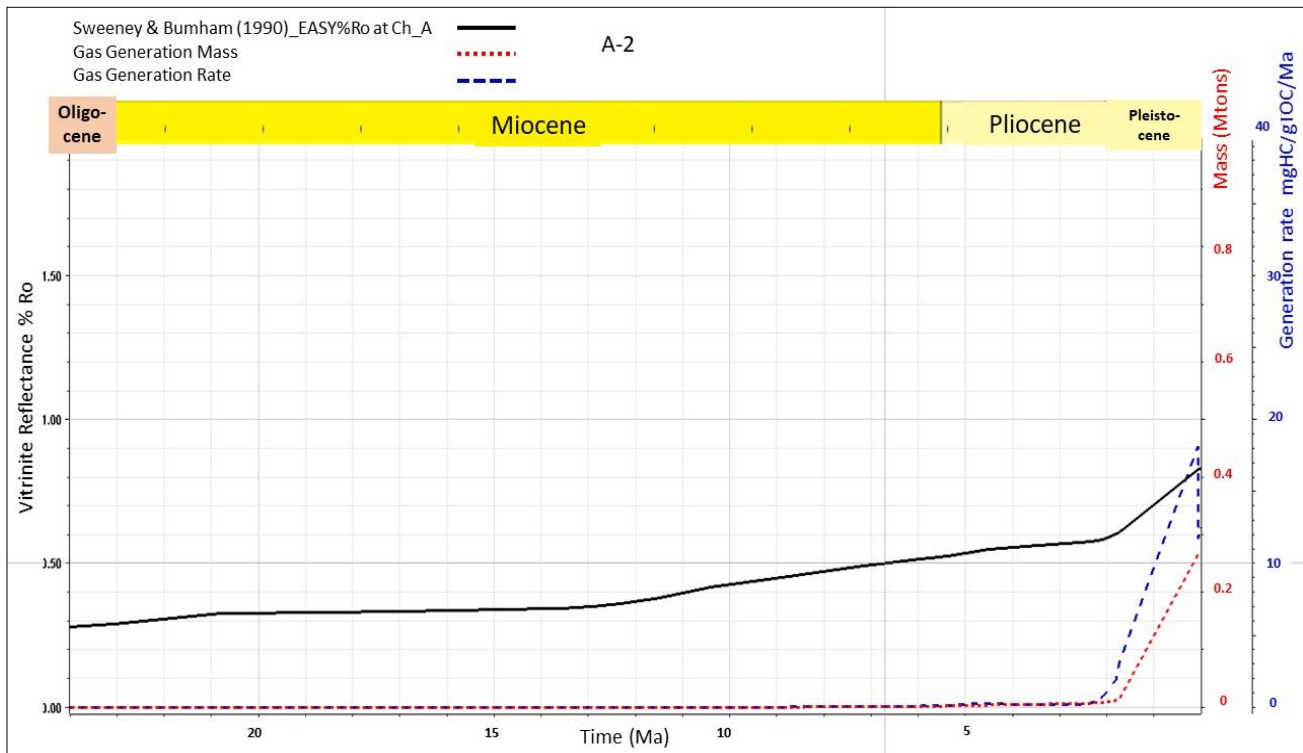
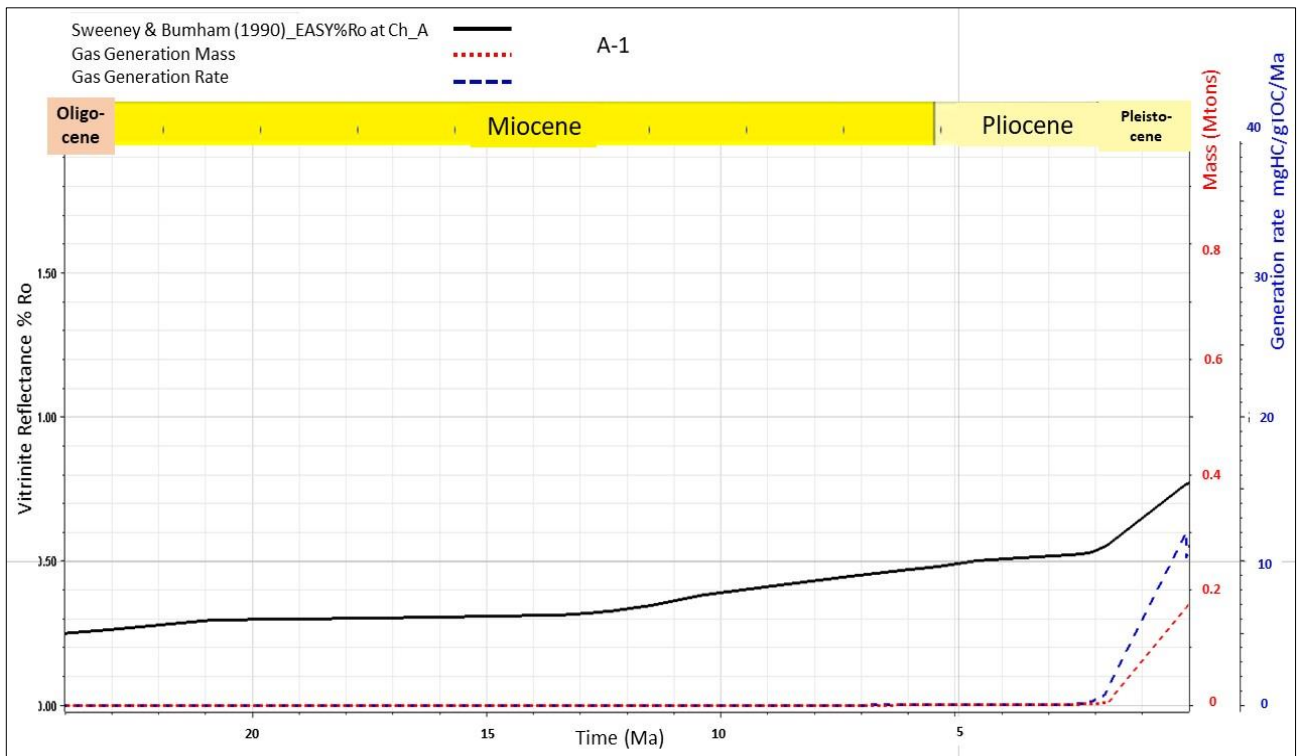


Fig. 7a. Ch_A source rock unit modeling for X-1 well, three curves identified Ro (solid curve), Generation Rate (dashed curve), and Generation Mass (pointed curve), within two subunits (A-1) for Ch_A_3 subunit and (A-2) for Ch_A_2 subunit.

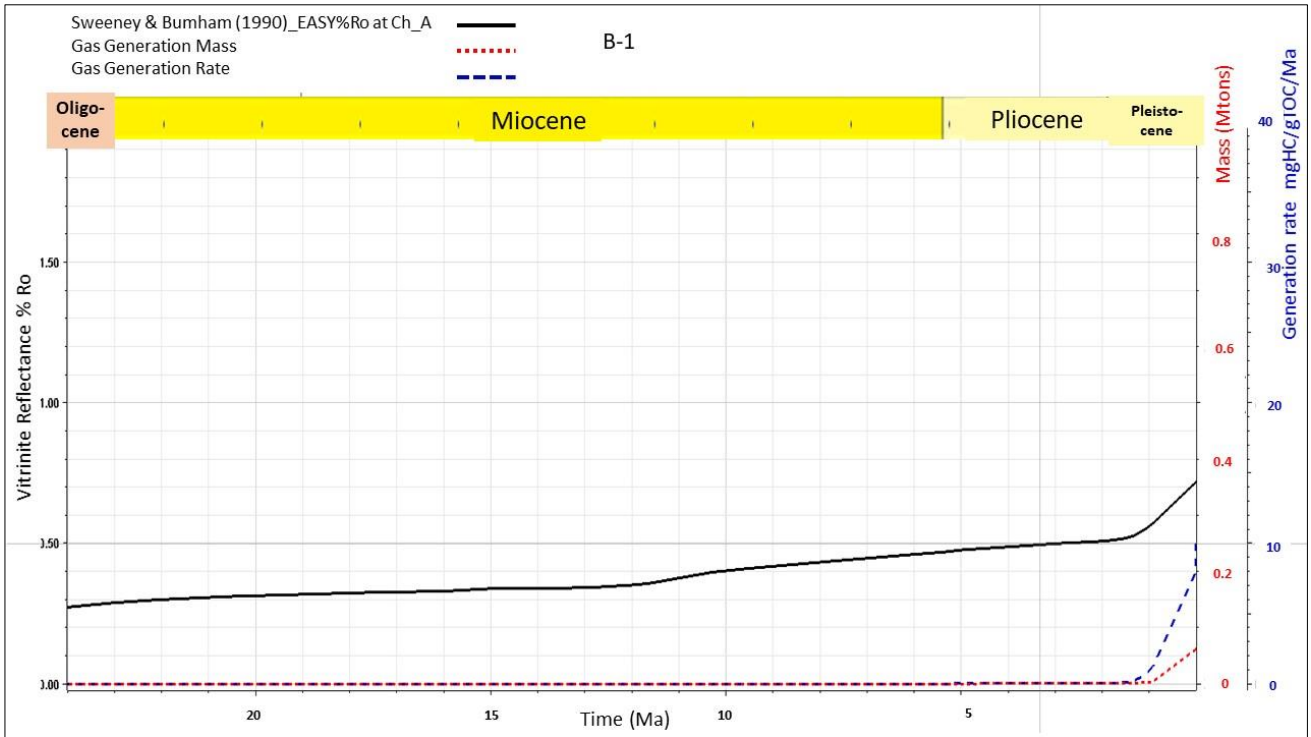


Fig. 8a. Ch_A source rock unit modeling for Salamat-1 well, three curves identified Ro (solid curve), Generation Rate (dashed curve), and Generation Mass (pointed curve). within (B-1) for Ch_A_3.

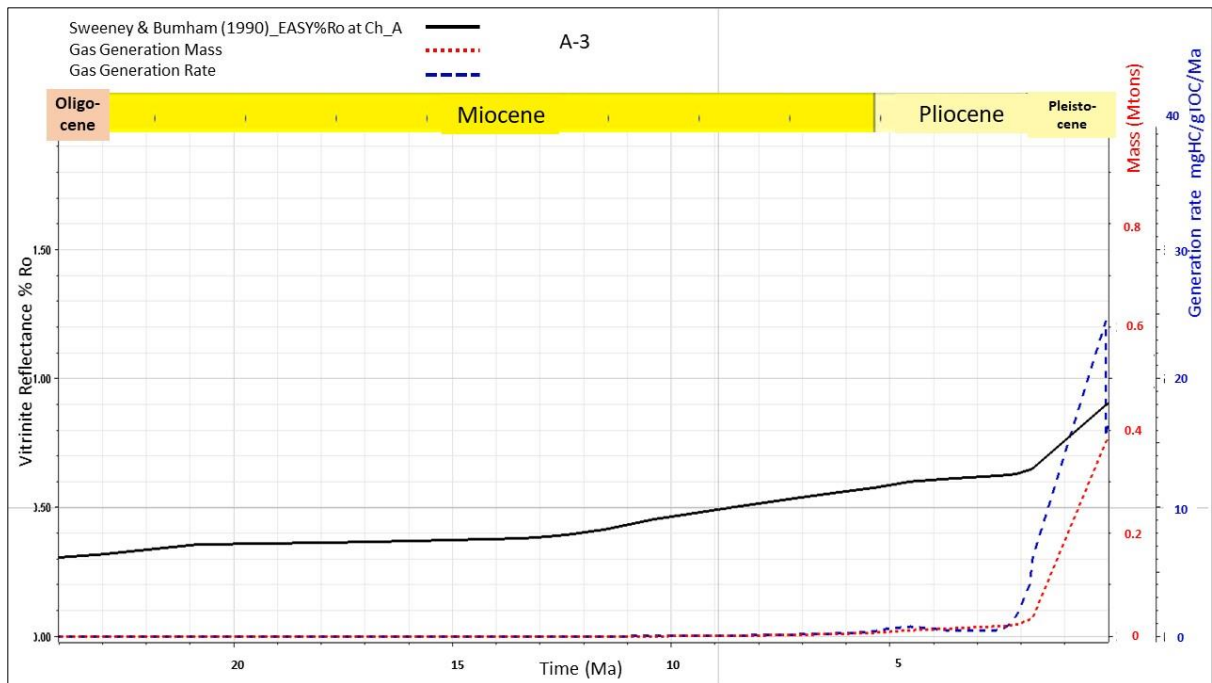


Fig. 7b. Ch_A source rock unit modeling for X-1 well, three curves identified Ro (solid curve), Generation Rate (dashed curve), and Generation Mass (pointed curve). within (A-3) Ch_A_1 subunit.

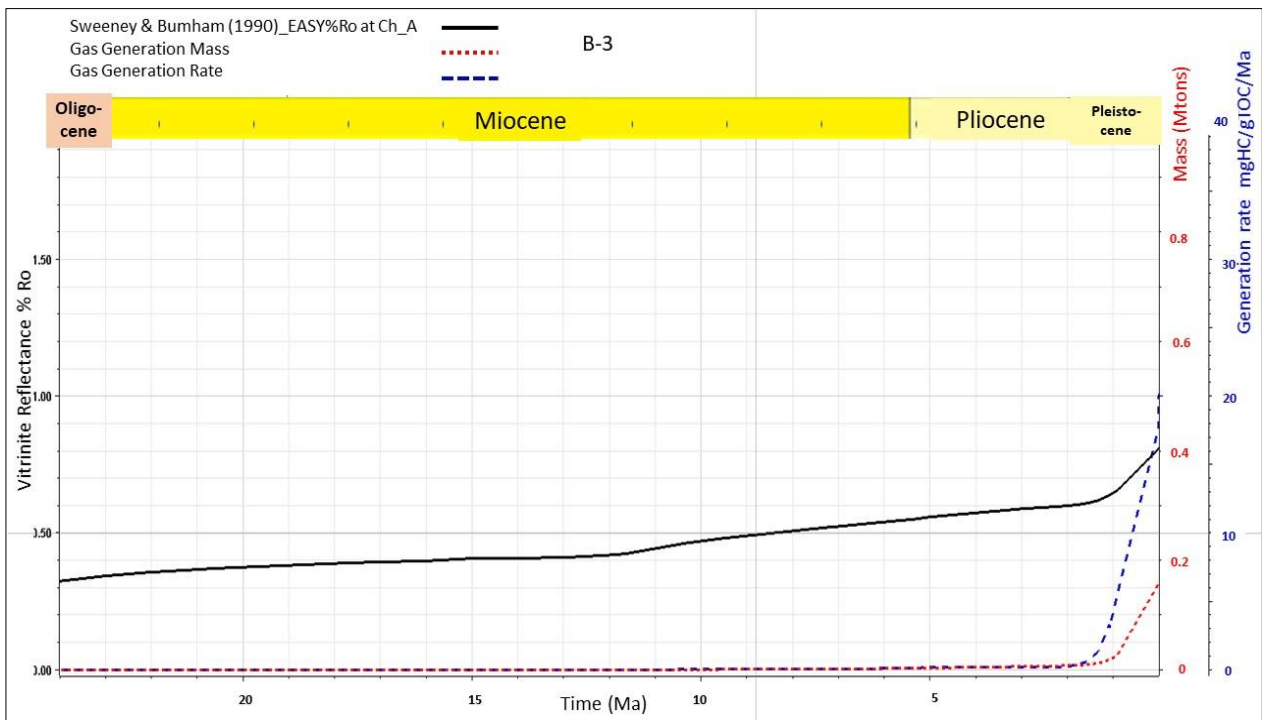
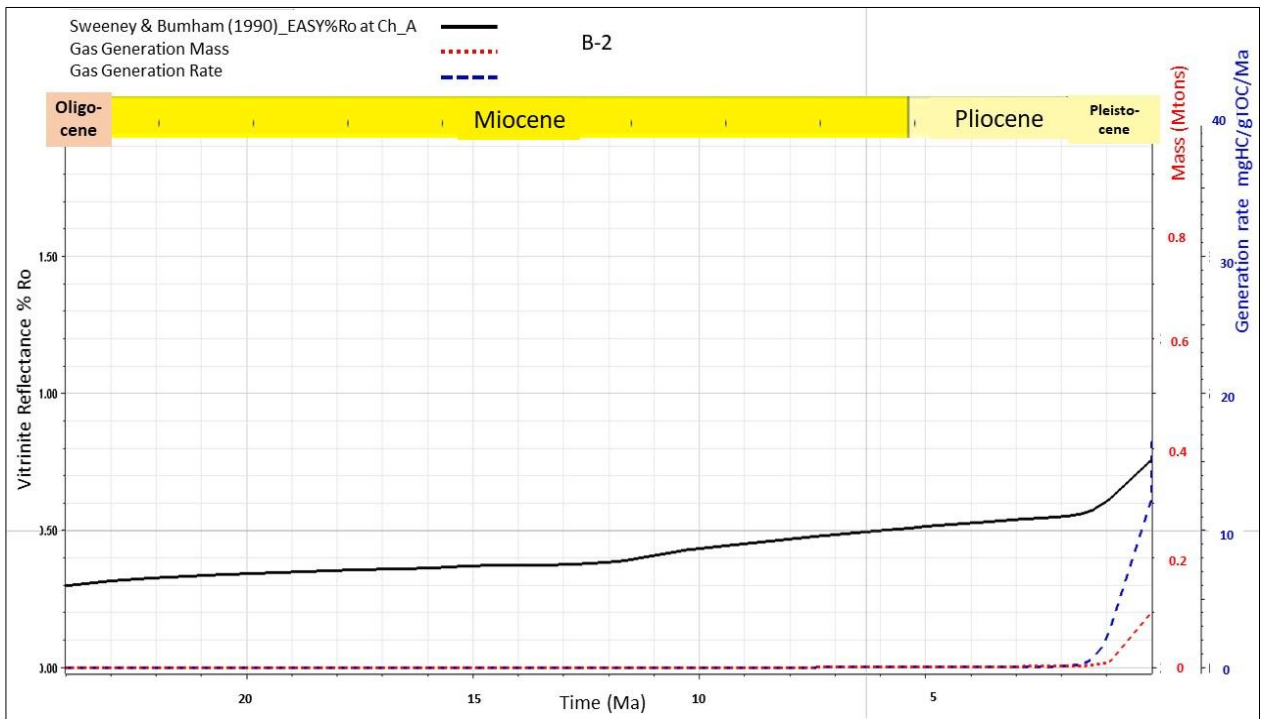


Fig. 8b. Ch_A source rock unit modeling for Salamat-1 well, three curves identified Ro (solid curve), Generation Rate (dashed curve), and Generation Mass (pointed curve), within two subunits (B-2) for Ch_A_2 subunit and (B-3) for Ch_A_1 subunit.

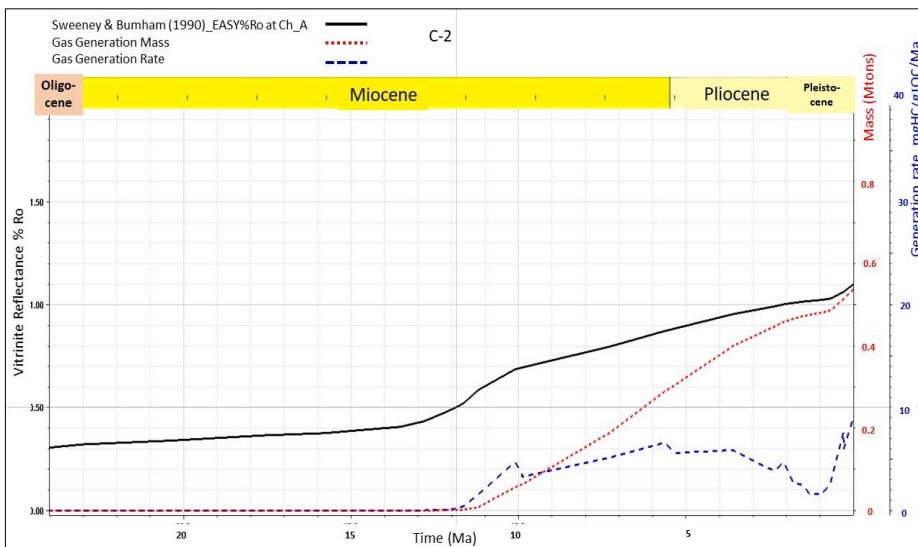
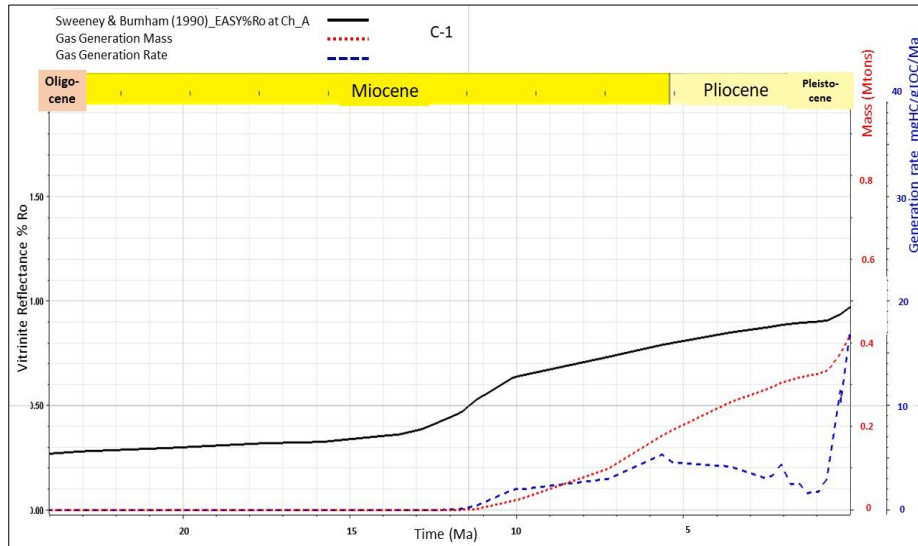


Fig. 9a. Ch_A source rock unit modeling for Notus-1st2 well, three curves identified Ro (solid curve), Generation Rate (dashed curve), and Generation Mass (pointed curve). within two subunits (C-1) for Ch_A_2 and (C-2) for Ch_A_1.

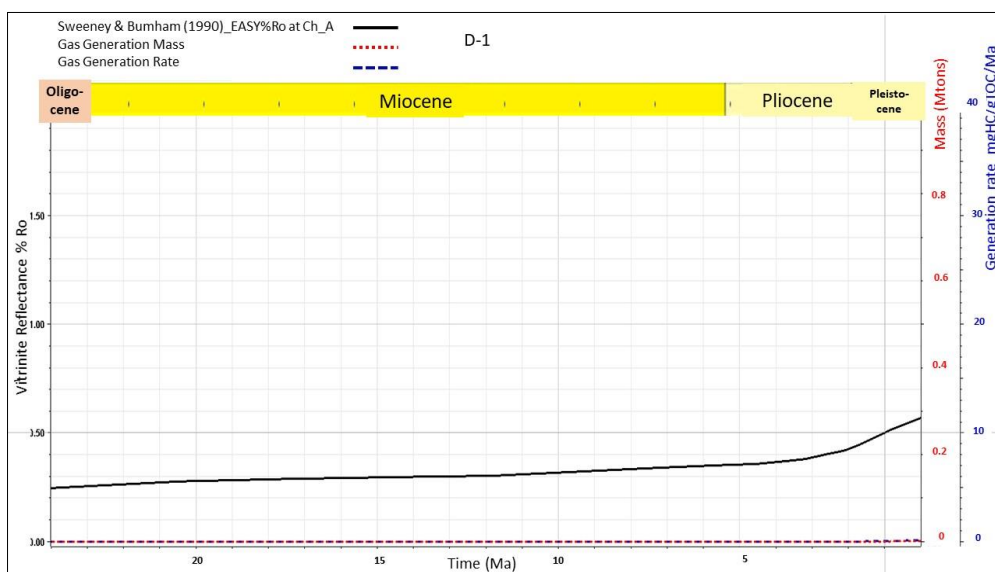


Fig. 9b. Ch_A source rock unit modeling for Helm-1st1well, three curves identified Ro (solid curve), Generation Rate (dashed curve), and Generation Mass (pointed curve). within (D-1 for Ch_A).

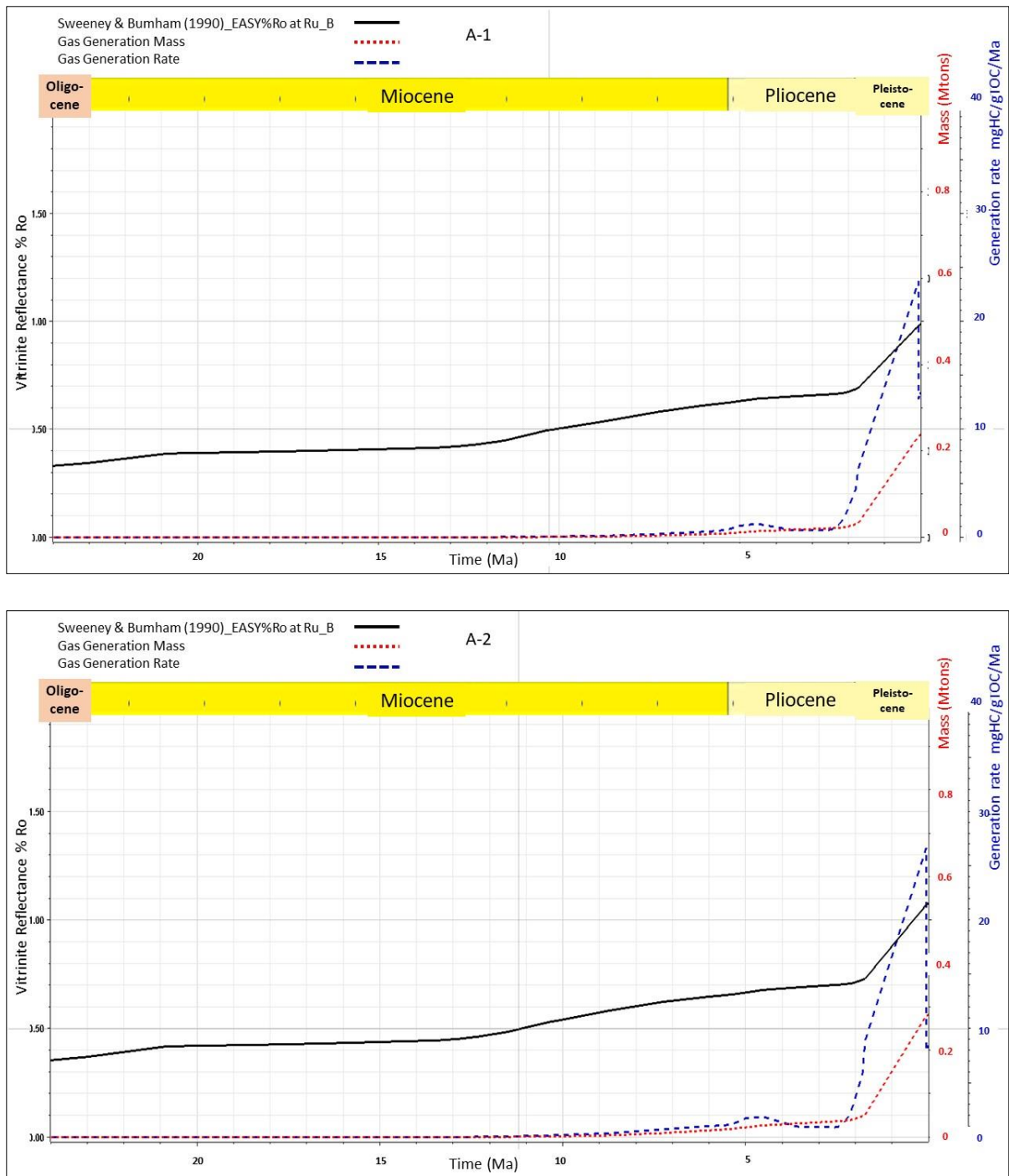


Fig. 10a. for Ru_B source rock unit modeling for X-1, three curves identified Ro (solid curve), Generation Rate (dashed curve), and Generation Mass (pointed curve). within two subunits (A-1) for Ru_B_2 and (A-2) for Ru_B_1.

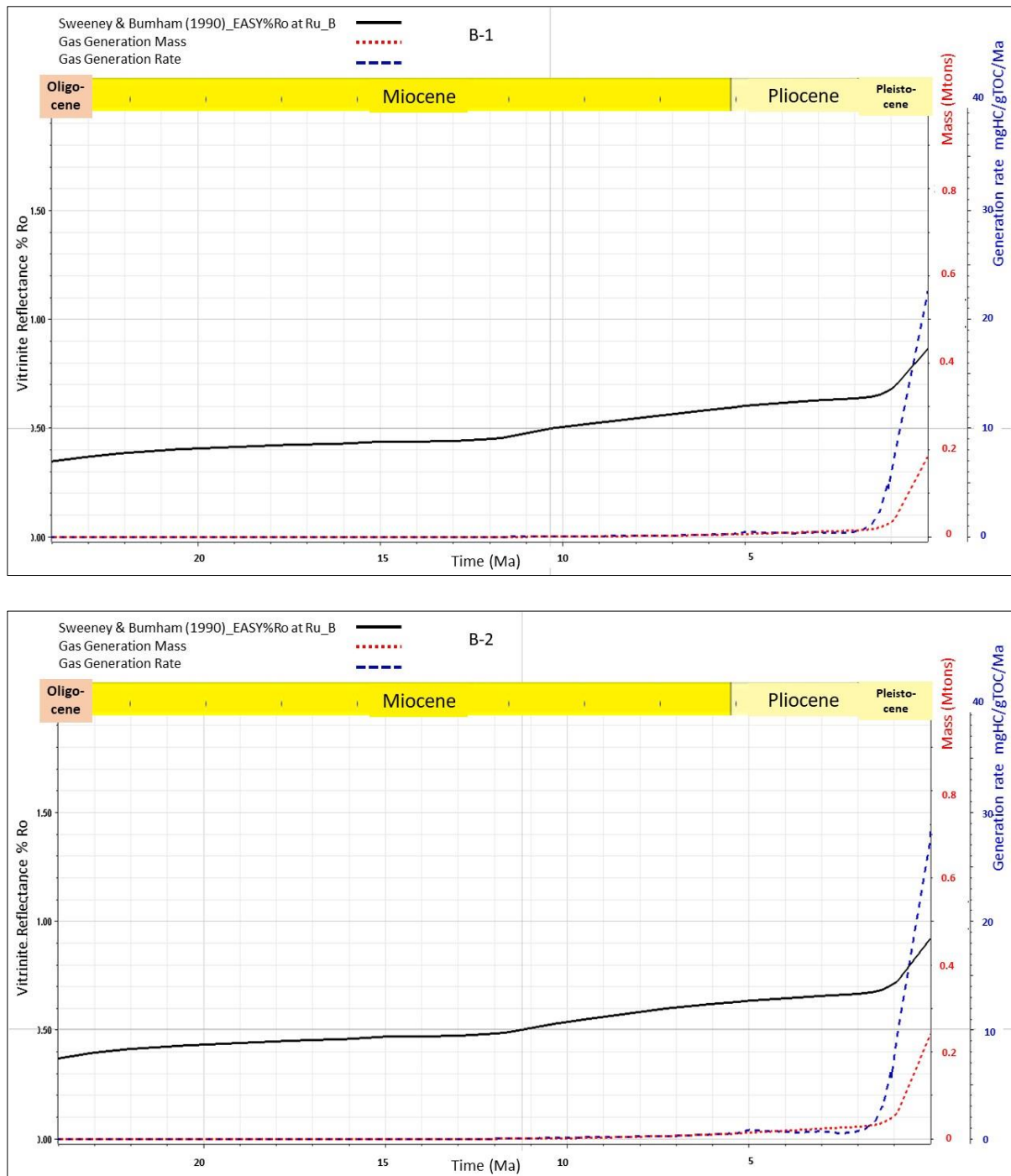


Fig. 10b. for Ru_B source rock unit modeling for Salamat-1 wells, three curves identified Ro (solid curve), Generation Rate (dashed curve), and Generation Mass (pointed curve), within two subunits (B-1) for Ru_B_2 and (B-2) for Ru_B_1.

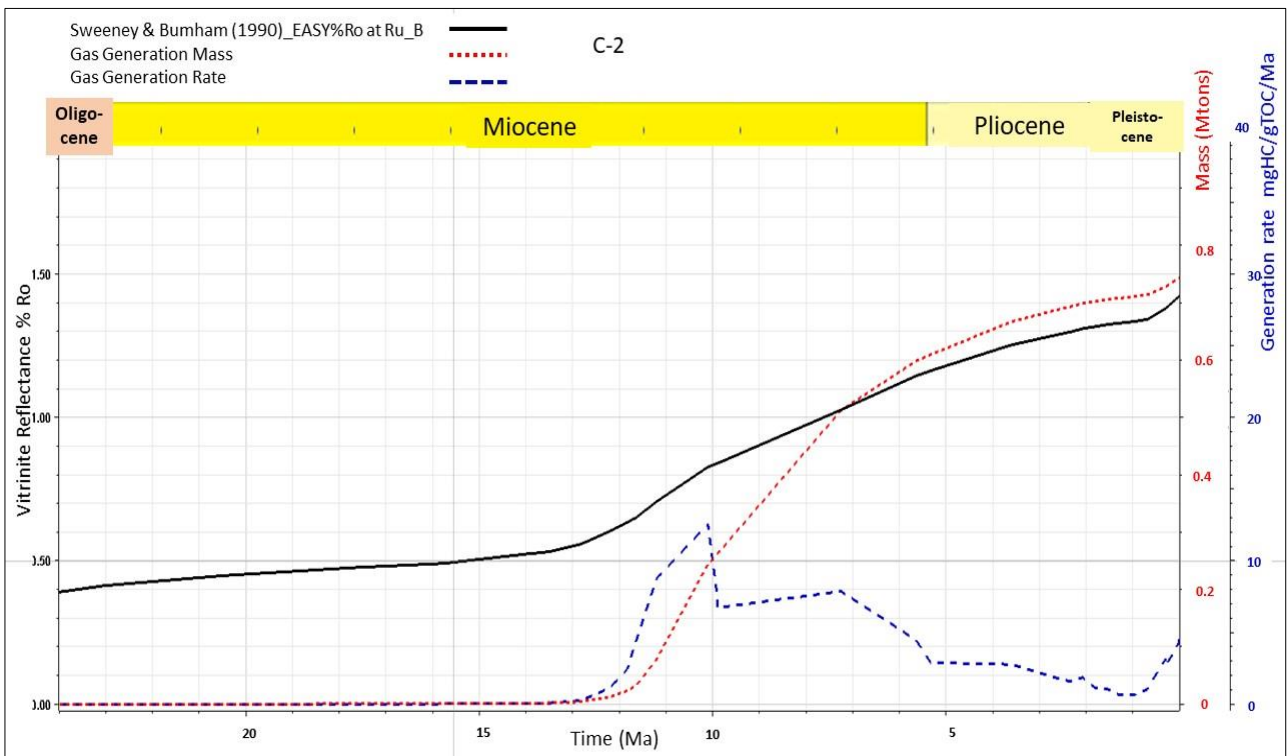
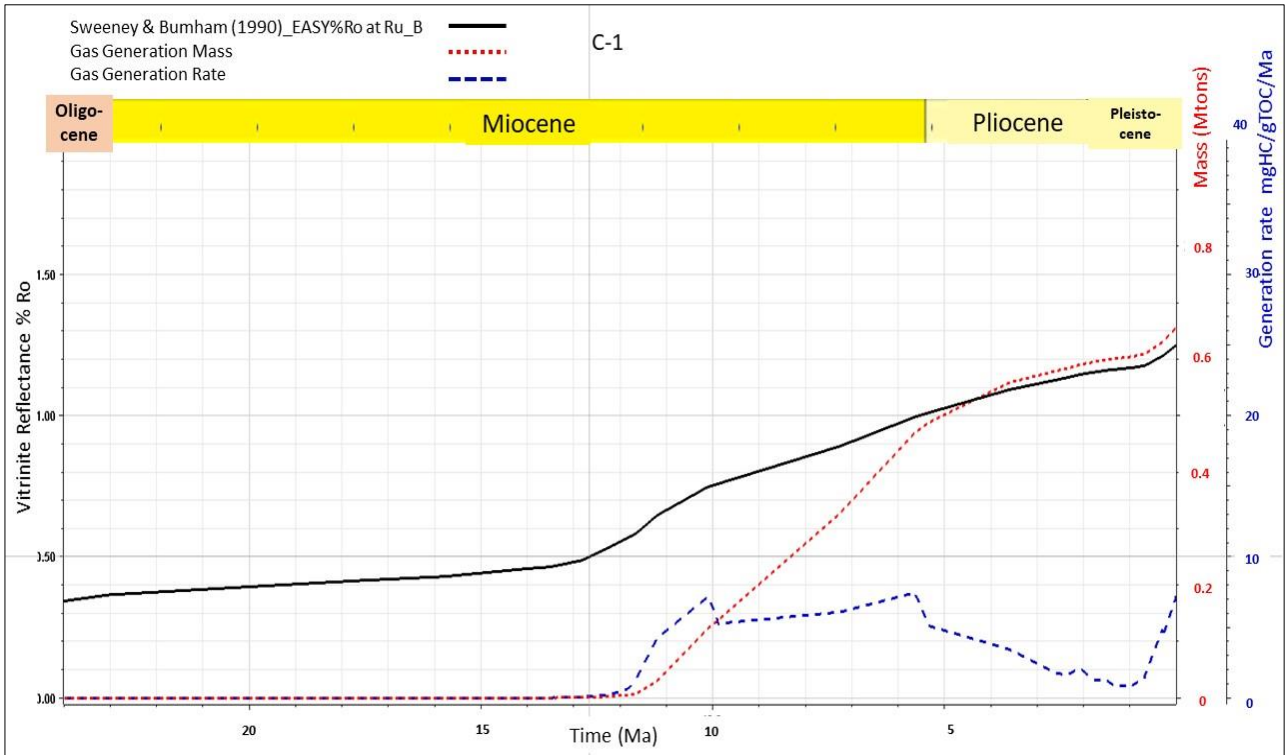


Fig. 11a. Ru_B source rock unit modeling for Notus-1st2 well three curves identified Ro (solid curve), Generation Rate (dashed curve), and Generation Mass (pointed curve), within two subunits (C-1) for Ru_B_2 and (C-2) for Ru_B_1.

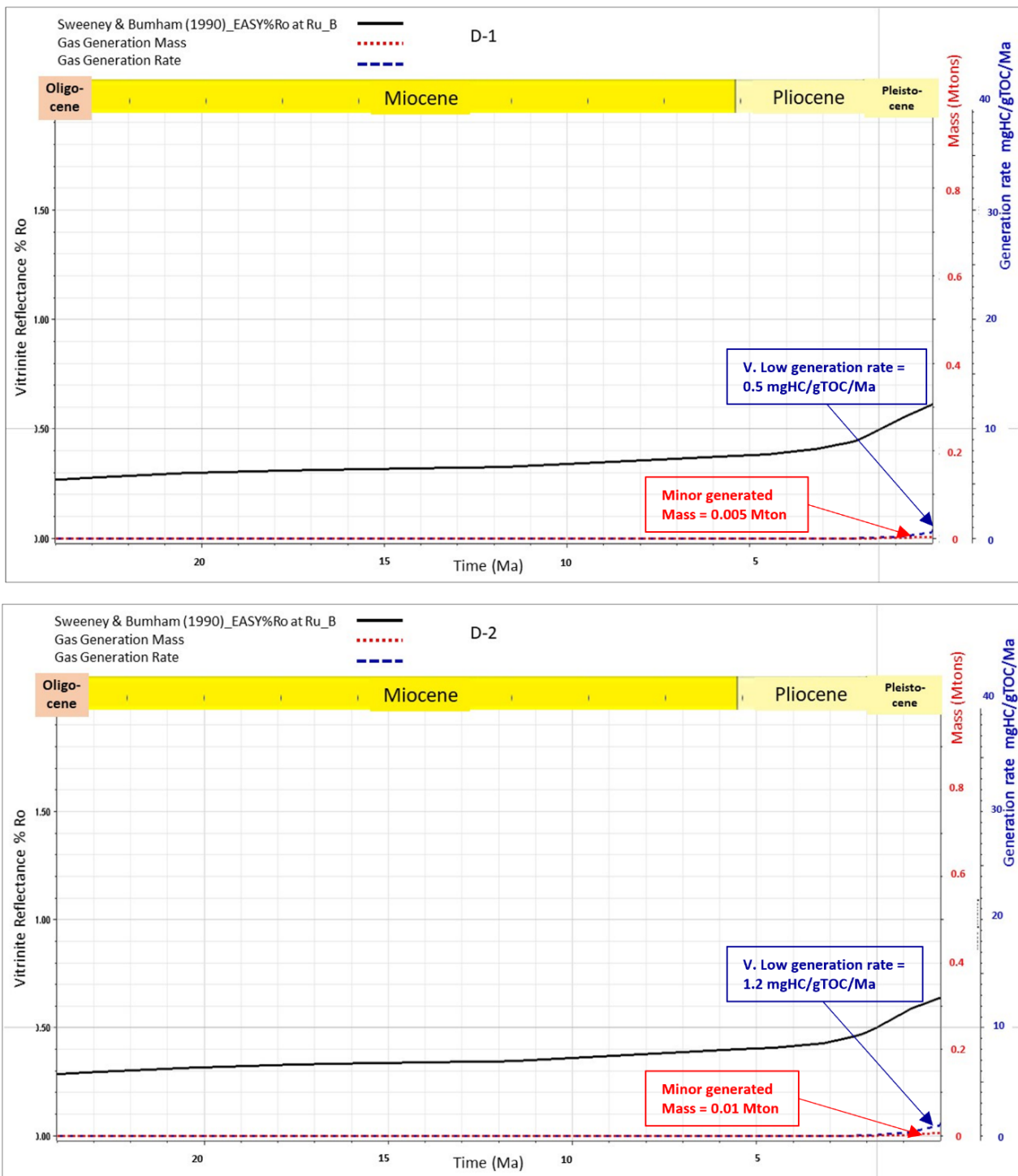


Fig. 11b. Ru_B source rock unit modeling for Helm-1st1 well three curves identified Ro (solid curve), Generation Rate (dashed curve), and Generation Mass (pointed curve). within two subunits (D-1) for Ru_B_2 and (D-2) for Ru_B_1.

4 Conclusion

- **Impact of Overburden and Compaction on Reservoir Quality:** The thickness of overburden rock and resulting compaction significantly influence porosity values. Sandstones of the same age and origin display variable porosity depending on burial depth. Reservoir quality generally improves toward the basin, correlating with the increased influence of turbidite channel systems that become more developed from the continental shelf to the slope.

- **Thermal Maturation and Hydrocarbon Generation:** Basin modeling has confirmed thermal maturation and thermogenic gas expulsion in three of the four studied wells. The evaluated Oligocene source rocks are sufficiently mature, capable of generating thermogenic gas, and show a mix of thermogenic and biogenic contributions. Maturity increases basinward, aligning with deeper burial and higher thermal exposure.

- **Source Rock and Reservoir Systems:** The Oligocene shales are identified as the primary source rocks for both Oligocene and Miocene reservoirs. Successful exploration efforts in the Rupelian and Chattian formations confirm the effectiveness of integrating structural and stratigraphic approaches. The widespread turbidite channel systems in the Nile Delta are key Oligocene reservoirs, with significant hydrocarbon potential.

- **Chronostratigraphic and Sequence Stratigraphy Insights:** The integration of chronostratigraphic correlation and sequence stratigraphy has allowed for the spatial and temporal mapping of these channel systems. 1D modeling confirms that the Oligocene source rocks (Rupelian and Chattian) have reached the gas maturity window, serving as the primary gas source. Minor contributions from Mesozoic source rocks in the form of low API condensates are also present.

- **Recommendations for Future Exploration:** Further exploration should integrate the results of this study with a detailed assessment of the regional structural and depositional framework to optimize hydrocarbon exploration and identify additional prospective targets.

- Within the studied wells:

- Notus-1st2 and X-1 should be prioritized for further exploration and detailed seismic and petrophysical analysis, given their strong hydrocarbon generation and favorable reservoir characteristics.
- Salamat-1 warrants additional evaluation for its potential in stratigraphic traps.
- The Helm-1st1 well has limited exploration potential and may serve more as a calibration point for regional geological modeling.

Acknowledgements: The authors are appreciating to thank the Egyptian Natural Gas Holding Company (EGAS) for permission to use and publish the data in this study and allowing access to the needed facilities and software.

Ethics Approval: The authors demonstrate a commitment to avoiding any misrepresentation of research findings that may have adverse effects on the reputation of the journal, the integrity of scientific authorship, and the overall scientific enterprise. The adherence to the parameters outlined in the journal's directives ensured the preservation of research integrity and the quality of its presentation, in accordance with the principles of sound scientific practice.

Conflicts of Interests: The authors have no conflicts of interest to declare that are relevant to the content of this article.

Author Contribution: All authors shared in writing, editing and revising the manuscript. Authors have read and agreed to the published version of the manuscript.

Funding: The authors did not receive support from any organization for the submitted work; the work depends on their own expenses.

Data Availability: The datasets generated and/or analyzed during the current study are not publicly available due to these data are owned exclusively by hydrocarbon exploration company, but are available from the corresponding author on reasonable request.

Consent to publish: All authors agreed with the content and that all gave explicit consent to submit and that they obtained consent from the responsible authorities at the institute/organization where the work has been carried out, before the work is submitted.

References

- Abdel Aal A., Price R.J., Vaitl J.D., and Shallow J.A., (1994). Tectonic evaluation of the Nile Delta, its impact on sedimentation and hydrocarbon potential. E.G.P.C. 12th Exploration and Production Conference 1 pp.19–34.
- Abdel-Fattah M.I., Sen S., Abuzied S.M., Abioui M., Radwan, A.E., and Benssaou M. (2022). Facies analysis and petrophysical investigation of the Late Miocene Abu Madi sandstones gas reservoirs from offshore Baltim East field (Nile Delta, Egypt). *Mar. Pet. Geol.*137(5), 105501.
- Asquith, G.B., (1982). Basic well log analysis for geologists. Published by AAPG. pp. 28-91.

- Attia, M. M. A., Farag, A. E.-S., & Zein El-Din, M. Y. (2024). Geomechanical study of rock properties in the Kafr El-Sheikh Formation at Sapphire Field, West Delta Deep Marine, Egypt. *Al-Azhar Bulletin of Science*, 35(2), Article 3.
- Barber P.M., (1981). Messinian subaerial erosion of the proto-Nile Delta. *Mar Geol.* 44 (3–4).253–272.
- Bentham P., (2011). Understanding crustal structure and the early opening history of the Eastern Mediterranean Basin, offshore Northern Egypt and the Levant. In: *New and Emerging Plays in the Eastern Mediterranean*, 23–25th February 2011, pp. 67–68. The Geological Society, Burlington House.
- Braaksma H., Proust J.N, Kenter J.A.M., Drijkoningen G.G., and Filippidou N., (2006). Sedimentological, petrophysical, and seismic characterization of an upper Jurassic shoreface-dominated shelf Margin (The Boulonnais, Northern France). *J Sediment Res* 76:175–199.
- Catuneanu O., Khalifa M.A., and Wanas H.A., (2006). Sequence stratigraphy of the Lower Cenomanian Bahariya Formation, Bahariya Oasis, Western Desert Egypt. *Sediment Geol* 190:121–137.
- El-Fakharani, A., & Abd El-Rahman, Y. (2020). Geochemical characterization of Messinian evaporites in the Nile Delta: Implications for hydrocarbon exploration. *Marine and Petroleum Geology*, 112, 104034.
- El-Sayed, A. M., & El Barkooky, A. (2023). Seismic stratigraphy and tectonic influence on sedimentation in the Nile Delta offshore, Egypt. *Geological Society, London, Special Publications*, 520(1), 141–156.
- Gargani J., and Rigollet C., (2007). Mediterranean Sea level variations during the Messinian salinity crisis. *Geophys Res Lett* 34(10).
- Guiraud R., and Bosworth W., (1999). Phanerozoic geodynamic evolution of northeastern Africa and the northwestern Arabian platform. *Tectonophysics* 315(1–4).73–104.
- Hakimi, M. H., Sumner, R. W., & Abdullah, W. H. (2021). 1D basin modeling of the Mahakam Delta, Indonesia: Implications for hydrocarbon generation and migration. *Journal of Asian Earth Sciences*, 220, 104945.
- Haq B.U., Hardenbol J., and Vail P.R., (1987). Chronology of the fluctuating sea levels since the Triassic. *science* Vol. 235, NO. 479306 MAR 1987: 1156-1167.
- Harms J.C., and Wray J.L., (1990). Nile Delta. In Said (Ed.) *The geology of Egypt* (pp. 329–343). AA.Balkema/ Rotterdam/ Brookfeld 1990. Henry S (2000) Pitfalls in synthetics. *Lead Edge* 19(6).604.
- Hassan, R. M., & Abdel-Fattah, M. I. (2023). Paleogeographic evolution of the Nile Delta during the Oligo-Miocene: Implications for hydrocarbon exploration. *Journal of African Earth Sciences*, 202, 104814.
- Ismail, M., Zein El Din, M. Y., Sabry, A., & Raslan, S. (2023). Integrated pore-pressure prediction workflow and influence on seal capacity using well-logs and seismic velocity, West Offshore Nile-Delta, Egypt. *Al-Azhar Bulletin of Science*, 34(3), Article 8.
- Leila M., Moscariello A., and Šegvić B., (2019). Depositional facies controls on the diagenesis and reservoir quality of the Messinian Qawasim and Abu Madi formations, onshore Nile Delta Egypt. *Geol J* 54(3).1797–1813.
- Leila M., Moscariello A., Kora M., Mohamed A., and Samankassou E., (2020). Sedimentology and reservoir quality of a Messinian mixed siliciclastic- carbonate succession, onshore Nile Delta Egypt. *Marine Pet Geol* 112:104076.
- Mitchum R.M, Vail P.R, and Thompson S., (1977). Seismic stratigraphy and global changes of sea level, Part 2: The depositional sequence as a basic unit for stratigraphic analysis. In CE Payton (Ed.), *Seismic stratigraphy—applications to hydrocarbon exploration*. American Association of Petroleum Geologists, Memoir 26, pp. 53–62.
- Nosjean N., Holeywell R., Pettingill H.S., Roden R., and Forrest M., (2021). Geological probability of success assessment for amplitude-driven prospects: a Nile Delta case study. *J.Pet.Sci. Eng.* 202, 108515 (2021).
- Posamentier H.W., and Vail P.R., (1988). Eustatic controls on clastic deposition II: Sequence and systems tract models. In CK Wilgus, BS Hastings, CGS C Kendall, HW Posamentier, CA Ross, & JC Van Wagoner (Eds.), *Sea-level changes: an integrated approach*. SEPM, Special Publication 42, pp. 125–154.
- Sachsenhofer, R. F., Tari, G., & Linzer, H. (2018). Thermal evolution and petroleum system analysis of the Western Black Sea Basin. *Journal of Petroleum Geology*, 41(2), 155–175
- Said R (1990). *The geology of Egypt*. AA.Balkema/ Rotterdam/ Brookfeld 1990 p.439-494.
- Schenk, C. J., Mercier, T. J., Finn, T. M., Woodall, C. A., Marra, K. R., Leathers-Miller, H. M., Le, P. A., & Drake, R. M. II. (2021). Assessment of undiscovered conventional oil and gas resources in the eastern Mediterranean area, 2020 (ver. 1.1). *U.S. Geological Survey Fact Sheet*, 2021–3032, 4 p.
- Sweeney J.J., and Burnham A.K., (1990). Evaluation of a simple model of vitrinite reflectance based on chemical kinetics. *AAPG Bull*74: 1559–1570.